SNARE mimicry by the CD225 domain of IFITM3 enables regulation of homotypic late endosome fusion

Kazi Rahman[1,#], Isaiah Wilt[1], Abigail A. Jolley[1], Bhabadeb Chowdhury[1], Siddhartha A. K. Datta[1], Alex A. Compton[1,*]

[1]HIV Dynamics and Replication Program, Center for Cancer Research, National Cancer Institute, Frederick, Maryland

[#]Present address: Department of Biochemistry and Microbiology, School of Health and Life Sciences, North South University, Dhaka, Bangladesh

[*]Corresponding author: alex.compton@nih.gov

Abstract

The CD225/Dispanins superfamily consists of membrane proteins that regulate vesicular transport and membrane fusion events driving neurotransmission, glucose transport, and antiviral immunity. However, how the CD225 domain controls membrane trafficking was unknown. We reveal that the CD225 domain contains a SNARE-like motif that enables interaction with cellular SNARE fusogens. Proline rich transmembrane protein 2 (PRRT2) encodes a SNARE-like motif that enables interaction with neuronal SNARE proteins, and mutations therein disrupt SNARE binding and are linked to neurological disease. Another CD225 member, interferon-induced transmembrane protein 3 (IFITM3), protects cells against Influenza A virus infection. IFITM3 interacts with SNARE proteins that mediate late endosome-late endosome (homotypic) fusion and late endosome-lysosome (heterotypic) fusion. IFITM3 binds to syntaxin 7 (STX7) in cells and in vitro, and mutations that abrogate STX7 binding cause loss of antiviral activity against Influenza A virus. Mechanistically, IFITM3 disrupts assembly of the SNARE complex controlling homotypic fusion and accelerates the trafficking of endosomal cargo to lysosomes. Our results suggest that SNARE modulation plays a previously unrecognized role in the diverse functions performed by CD225 proteins.

Introduction

Membrane fusion is a critical process enabling cargo transfer between membrane-bound compartments. The soluble NSF attachment protein receptor (SNARE) proteins are key mediators of membrane fusion and are involved in nearly every vesicular trafficking event in eukaryotic cells (Hong, 2005; Jahn & Scheller, 2006). SNARE proteins contain a so-called SNARE motif consisting of heptad repeats of generally hydrophobic amino acids surrounding a central hydrophilic residue (R for arginine or Q for glutamine) (Fasshauer *et al*, 1998). The central residue is referred to as the “0” layer while the hydrophobic residues surrounding it are numbered relative to the “0” layer, from “-7” to “+8” (**Figure 1A**). These features enable the assembly of four parallel alpha-helices (one R-SNARE motif and three Q-SNARE motifs) into a coiled-coil trans-SNARE complex across two membranes. Progressive folding of the bundle towards a cis-SNARE complex, in which the SNARE proteins reside within the same membrane, drives membrane fusion (Han *et al*, 2017). Humans encode a minimum of 38 SNARE proteins

which interact selectively to impart specificity and directionality to membrane fusion events between different organelles (Kloepper *et al*, 2007).

Among the best studied are the synaptic SNARE proteins that mediate the exocytosis of neurotransmitters from neurons (Sudhof, 2004). Neurotransmitter release at neuronal synapses requires the fusion of synaptic vesicles with the presynaptic plasma membrane, and this requires the assembly of syntaxin 1A and SNAP-25 (in the presynaptic plasma membrane) with VAMP2 (in the synaptic vesicle membrane) (Sutton *et al*, 1998; Xiao *et al*, 2001). The study of neurological diseases associated with impaired neurotransmission has led to the identification of cellular proteins that regulate synaptic SNARE assembly, such as proline-rich transmembrane protein 2 (PRRT2) (Ebrahimi-Fakhari *et al*, 2015). Mutations in PRRT2 associated with a range of neurological disorders in humans (including paraoxysmal kinesigenic dyskinia (PKD), infantile epilepsy and convulsions, hemiplagic migraines, ataxia, and intellectual disability) indicated that PRRT2 plays important roles in neurotransmission (Ebrahimi-Fakhari *et al*., 2015). Subsequently, it was shown that PRRT2 interacts with Q-SNAREs syntaxin 1A and SNAP-25 and disfavors their interaction with the R-SNARE VAMP2, thereby reducing synaptic SNARE assembly and neurotransmitter release (Coleman *et al*, 2018; Ma *et al*, 2018; Tan *et al*, 2018; Valente *et al*, 2016). However, a comprehensive understanding of the protein-protein interface enabling this regulatory function of PRRT2 was unknown. PRRT2 belongs to the CD225 superfamily, a group that includes trafficking regulator of GLUT4 (TRARG1/TUSC5) and interferon-induced transmembrane protein 3 (IFITM3) (Coomer *et al*, 2021). TUSC5 and IFITM3 regulate vesicular trafficking during glucose transport and virus infection, respectively, through incompletely understood mechanisms. IFITM3 provides constitutive and interferon-induced protection of cells from endocytic viruses such as Influenza A virus (IAV) by homing to virus-containing endosomes and inhibiting virus-cell membrane fusion, effectively preventing the delivery of the viral core into host cell cytosol (where virus replication begins) (Desai *et al*, 2014; Klein *et al*, 2023; Li *et al*, 2013; Suddala *et al*, 2019). Moreover, *Ifitm3* knockout mice and disease-associated single-nucleotide polymorphisms in human *IFITM3* revealed that IFITM3 prevents severe viral disease sequelae in vivo (Bailey *et al*, 2012; Everitt *et al*, 2012).

Here, we report the identification of an R-SNARE-like motif shared among many CD225 family members that enables SNARE binding and modulation of SNARE assemblies. Mutation of residues within the R-SNARE-like motif of PRRT2, TUSC5, and IFITM3 resulted in reduced Q-SNARE binding and loss of their respective functions, as demonstrated experimentally or by associations with human disease. In-depth analysis revealed that IFITM3 interacts with endosomal SNARE proteins and, as a result, inhibits the assembly of the SNARE complex mediating homotypic late endosome fusion. Our findings suggest that cells expressing IFITM3 prioritize the heterotypic fusion pathway whereby late endosomes fuse with lysosomes, resulting in endosomal cargo degradation. Our findings demonstrate that CD225 proteins regulate diverse membrane trafficking processes in different tissues by regulating cellular fusion machinery via a conserved R-SNARE-like motif.

Results

To investigate whether the known SNARE-binding activity exhibited by human PRRT2 may be attributed to the presence of a previously unrecognized SNARE-like motif, we performed multiple protein sequence alignment between PRRT2 and a panel of Q- and R-SNARE proteins. We found that PRRT2 encodes an arginine that aligns with the central arginines present within

canonical R-SNARE motifs, which are approximately 53 amino acids in length (**Figure 1A**). Furthermore, like canonical R-SNARE proteins, PRRT2 contains regularly spaced, generally hydrophobic residues extending on both sides of the central arginine. Therefore, PRRT2 contains a putative R-SNARE motif, resembling that which is present in VAMP proteins. Importantly, we also found this R-SNARE-like motif in additional members of the human CD225 protein family, including IFITM1, IFITM2, IFITM3, IFITM5, IFITM10, TUSC5, although the identity and number of hydrophobic layers surrounding the central arginine varied between members (**Figure 1**). The central arginine was lacking in a subset of CD225 family members (**Figure EV1A**), suggesting either that the R-SNARE-like motif does not trace its origins to the CD225 ancestor or that the motif was lost to decay in certain family members.

Next, since PRRT2 has been described to regulate the SNARE complex controlling neurotransmission (Coleman *et al.*, 2018), we measured whether the R-SNARE-like motif present within PRRT2 confers it with the ability to bind neuronal SNARE proteins. In agreement with previous reports, ectopic PRRT2 co-immunoprecipitated with ectopic Q-SNARE SNAP-25 (**Figure 1B**). Attesting to a critical role played by the R-SNARE-like motif of PRRT2 in mediating this interaction, mutation of the central arginine (R295Q) resulted in decreased co-immunoprecipitation between PRRT2 and SNAP-25 (**Figure 1B**). Furthermore, mutation of one of the hydrophobic layers of the R-SNARE-like motif of PRRT2 (A320V) also abrogated the interaction with SNAP-25, and a G305W mutation that is adjacent to a hydrophobic layer and which inhibits PRRT2 homodimerization (Rahman *et al*, 2020) also abrogated this interaction (**Figure 1B**). Meanwhile, these mutations in PRRT2 did not affect the interaction between PRRT2 and another Q-SNARE in the neuronal SNARE complex, syntaxin 1A (**Figure EV1B**). Importantly, all three mutations (R295Q, G305W, and A320V) in PRRT2 occur naturally as polymorphisms in humans and are linked to neurological dysfunction (Becker *et al*, 2013; Ma *et al.*, 2018; Tan *et al.*, 2018). Therefore, our results describing an R-SNARE-like motif in human PRRT2 provide a mechanistic basis for the previously described molecular interaction between PRRT2 and neuronal SNARE proteins, as well as an explanation for how R295Q, G305W, and A320V cause loss of PRRT2 function in vivo and neurological dysfunction.

TUSC5 is a CD225 family member expressed in adipose tissue and implicated in the translocation of glucose transporter type 4 (GLUT4) to the cell surface, a process essential for insulin-stimulated glucose transport (St-Denis & Cushman, 1998; Stöckli *et al*, 2011). It was previously reported that TUSC5 co-immunoprecipitated with GLUT4 and SNARE proteins implicated in the vesicular trafficking of GLUT4 (Beaton *et al*, 2015; Fazakerley *et al*, 2015). However, the basis for this interaction was unknown. Like the CD225 family member PRRT2, TUSC5 also encodes a putative R-SNARE-like motif (**Figure 1A**). Accordingly, we found that ectopic TUSC5 co-immunoprecipitated with ectopic syntaxin 4, a Q-SNARE involved in GLUT4 translocation, while a G141W mutation in TUSC5 (analogous to G305W in PRRT2) disrupted this interaction (**Figure EV1C**). Reverse co-immunoprecipitation confirmed this finding (**Figure EV1D**). Collectively, these results highlight the presence of a R-SNARE-like motif in CD225 family members that enables coordination of SNARE proteins involved in diverse membrane fusion processes.

The IFITM proteins IFITM1, IFITM2, and IFITM3 are among the best characterized members of the CD225 protein family due to their established roles in cell-intrinsic defense against diverse pathogenic viruses (Majdoul & Compton, 2021; Shi *et al*, 2017). IFITM2 arose through gene duplication of IFITM3 in the ancestor of great apes, and both IFITM2 and IFITM3 proteins accumulate in membranes of the endolysosomal compartment (Compton *et al*, 2016). In

addition to preventing virus escape from the endocytic compartment, it has been demonstrated that IFITM3 redirects incoming virions to lysosomes for degradation (Feeley *et al*, 2011; Spence *et al*, 2018; Suddala *et al.*, 2019). However, the mechanism for this latter effect by IFITM3 was unknown, as was its relevance to the antiviral activity exhibited by IFITM3. Since IFITM3 is an endolysosomal protein, we assessed whether the R-SNARE-like motif in IFITM3 (**Figure 1A**) conferred IFITM3 with the ability to bind and regulate endolysosomal SNARE proteins.

Fusion between compartments of the endolysosomal system are controlled by SNARE complexes consisting of the Q-SNAREs syntaxin 7 (STX7), syntaxin 8 (STX8), Vti1b, and one of two R-SNAREs—VAMP8 or VAMP7 (**Figure 2A**). The STX7-STX8-Vti1b-VAMP8 complex enables late endosome-late endosome (homotypic) fusion while the STX7-STX8-Vti1b-VAMP7 complex is responsible for late endosome-lysosome (heterotypic) fusion (Advani *et al*, 1999; Mullock *et al*, 2000; Prekeris *et al*, 1999; Pryor *et al*, 2004). Endocytic viruses like IAV exploit the endolysosomal network and the SNARE machinery found therein in order to avoid lysosomal degradation and gain access to host cell cytosol, where virus replication is initiated. VAMP8 and its role in late endosome homotypic fusion was previously reported to promote IAV entry into cells. In contrast, VAMP7 inhibited IAV entry, presumably by favoring the degradation of virus-laden late endosomes with lysosomes (Pirooz *et al*, 2014a; Pirooz *et al*, 2014b). Therefore, we tested whether IFITM3 and the R-SNARE-like motif found in its CD225 domain could influence the assembly of SNARE complexes regulating the endolysosomal network.

The R-SNARE-like motif is conserved among the interferon-inducible members of the human IFITM family that exhibit antiviral activity—IFITM1, IFITM2, and IFITM3 (**Figure 2A**). In contrast to a canonical R-SNARE protein like VAMP8, the R-SNARE-like motif of IFITM1-3 lack two layers of hydrophobicity at the amino-terminal end of the motif. Instead, IFITM1-3 encode an amphipathic helix that was shown to mediate cholesterol binding activity, membrane binding, and which is essential for antiviral activity against IAV (Chesarino *et al*, 2017; Guo *et al*, 2021; Rahman *et al.*, 2020; Rahman *et al*, 2022) (**Figure 2A**). Interestingly, the intact hydrophobic layers forming part of the R-SNARE-like motif downstream of the amphipathic helix include residues that were previously shown to be important for antiviral activity: a cysteine residue previously shown to be palmitoylated (Chesarino *et al*, 2014; Hach *et al*, 2013; Yount *et al*, 2010) and two phenylalanine residues shown to be critical for antiviral function(John *et al*, 2013; Suddala *et al.*, 2019) (**Figure 2A**). Therefore, to provide further evidence that the R-SNARE-like motif of IFITM3 contributes functionally to its antiviral activity, we assessed how mutation of the central arginine (R85Q) or the two phenylalanines (F75A/F78A) impacted antiviral activity against IAV. We also tested the effect of mutating glycine 95 (G95L), since it is adjacent to a hydrophobic layer in the R-SNARE-like motif of IFITM3, is homologous to glycine 305 in PRRT2 and glycine 141 in TUSC5 (**Figure 1B and Figure EV1C and EV1D**), and was previously shown by us to be critical for antiviral activity (Rahman *et al.*, 2020). While IFITM3 WT reduced IAV infection by approximately 80% relative to Empty Vector, all mutants tested exhibited a near-total loss of antiviral activity (**Figure 2B**). These results indicate that the antiviral activity of IFITM3 against IAV depends upon a previously uncharacterized R-SNARE-like motif. Furthermore, our findings suggest that interactions with SNARE machinery may comprise an essential but unrecognized component of IFITM3 function in cells.

Next, we addressed whether the R-SNARE-like motif of IFITM3 adopts a protein fold resembling that of a genuine R-SNARE. Since the atomic structure of IFITM3 is incompletely understood (Ling *et al*, 2016) and the influence of interaction partners on its structure has not been explored, we used the TM-align platform (Zhang & Skolnick, 2005) to perform protein

structure alignment between the R-SNARE-like motif of IFITM3 and the R-SNARE motif of VAMP8. The results supported that IFITM3 and VAMP8 adopt a highly similar alpha helical fold in the region spanning their respective R-SNARE motifs (TM-score = 0.76) (**Figure EV2A**). To further investigate the SNARE-like structural qualities of IFITM3, we used Alphafold (Mirdita *et al*, 2022; Varadi *et al*, 2024) and the flexible protein structure alignment algorithm FATCAT (Li *et al*, 2020) to model the R-SNARE-like motif of IFITM3 against a template consisting of the R-SNARE motif of VAMP8, which was previously crystallized in the context of the STX8-STX7-Vti1b-VAMP8 complex (Antonin *et al*, 2002). We found that the Alphafold model for the R-SNARE-like motif of IFITM3 exhibited a high degree of structural homology with the R-SNARE motif of VAMP8 (**Figure 2C**). We also swapped VAMP8 for IFITM3 in the context of the STX7-STX8-Vti1b-VAMP8 complex to provide spatial orientation of the F75, F78, and R85 residues of IFITM3. We found that the side chains of F75, F78, and R85 are predicted to radiate towards the center of the coiled-coil structure formed by Q-SNAREs STX7, STX8, and Vti1b (**Figure EV2B**). Moreover, the central arginine (R85) of IFITM3 is predicted to align with the central glutamine (Q) residues of STX7, STX8, and Vti1b (**Figure EV2C**). Therefore, IFITM3 encodes an R-SNARE-like motif that is predicted to behave like an endosomal R-SNARE protein.

To determine whether the R-SNARE-like motif of IFITM3 confers it with the ability to bind endolysosomal SNARE proteins in cells, we overexpressed IFITM3 in combination with individual endolysosomal SNARE proteins in HEK293T cells and performed co-immunoprecipitation. We found that IFITM3 immunoprecipitated from transfected cells pulled down relatively high quantities of ectopic STX7, while other endolysosomal SNARE proteins were pulled down to a lesser, or negligible, extent (**Figure 2D**). This selective co-immunoprecipitation between IFITM3 and STX7 was not due to elevated STX7 levels in transfected cells (**Figure 2D**). Importantly, mutations in IFITM3 that caused loss of antiviral function (F75/78A, R85Q, and G95L) (**Figure 2B**) diminished binding with STX7 relative to WT (**Figure 2E**). IFITM3 F75/78A and R85Q exhibited somewhat decreased steady-state levels relative to WT, possibly attesting to the importance of the R-SNARE-like motif in maintaining proper folding and stability of the IFITM3 polypeptide (**Figure 2E**). The association between IFITM3 and STX7 was confirmed by reverse co-immunoprecipitation, whereby immunoprecipitated ectopic STX7 pulled down ectopic IFITM3 (**Figure 3A**). Ectopic STX8 also co-immunoprecipitated with IFITM3 but to a lesser extent than STX7 (**Figure 3A**). To further support an association between IFITM3 and STX7, we performed confocal immunofluorescence in intact cells transfected with ectopic IFITM3 and STX7-GFP. We observed colocalization between IFITM3 WT and STX7-GFP, while IFITM3 G95L exhibited decreased colocalization (**Figure 3B**). These results demonstrate that an R-SNARE-like motif in IFITM3 enables it to bind to endosomal SNARE proteins, particularly Q-SNAREs STX7 and STX8. Furthermore, there exists a functional requirement for the R-SNARE-like motif of IFITM3 during restriction of IAV infection.

While our results are suggestive of selective binding between IFITM3 and Q-SNAREs STX7 and STX8, we also detected pull down of VAMP8-HA when IFITM3 was immunoprecipitated (**Figure 2D**). To confirm this interaction, we performed the reverse co-immunoprecipitation and found that VAMP8-HA pulled down IFITM3 WT, while pulldown was reduced by the G95L mutation (**Figure EV3A**). We also immunoprecipitated VAMP7-Myc and assessed pull down of ectopic IFITM3, because a previously published proteomic dataset identified VAMP7 as a possible binding partner of IFITM3 (Li *et al*, 2024). As was observed for

VAMP8-HA, VAMP7-Myc pulled down IFITM3 WT, while IFITM3 G95L was pulled down to a lesser extent (**Figure EV3B**). Together, these results suggest that ectopic IFITM3 can interact with endosomal Q-SNAREs as well as the R-SNAREs VAMP8 and VAMP7.

We then assessed whether endogenous IFITM3 exhibits SNARE binding activity. Following transfection of ectopic STX7 into HeLa WT or *IFITM3* KO cells, we found that ectopic STX7 pulled down endogenous IFITM3 (**Figure 4A**). As a control, pull down of endogenous IFITM3 by ectopic STX7 was lost in *IFITM3* KO cells (**Figure 3A**). *IFITM3* KO was specific, as IFITM2 protein levels were unaffected, and did not influence the overall levels of endolysosomal SNARE proteins (**Figure EV4A**). Moreover, the presence or absence of IFITM3 did not affect the co-immunoprecipitation between STX7 and other Q-SNAREs STX8 and Vti1b (**Figure EV4B**). We were unable to detect or immunoprecipitate endogenous STX7 in HeLa cells. However, we succeeded in immunoprecipitating endogenous STX8 and found that it pulled down endogenous IFITM3 (**Figure 4B**). Additionally, endogenous IFITM3 was also pulled down by endogenous Vti1b, VAMP8, and VAMP7 (**Figure 4C-4E**). These results demonstrate that endogenous IFITM3 binds to endolysosomal Q- and R-SNAREs in a direct or indirect manner. To determine whether IFITM3 can bind SNARE proteins directly, we produced and purified recombinant IFITM3 (**Figure EV4C and EV4D**) and incubated it with recombinant STX7 *in vitro* (**Figure EV4E and EV4F**). Immunoprecipitation of recombinant STX7 from the reaction resulted in pull down of recombinant IFITM3 WT, but this interaction was lost for IFITM3 F75/78A or IFITM3 G95L (**Figure 4F**). With size exclusion chromatography, we ruled out that the selective pull down of IFITM3 WT by recombinant STX7 was due to a tendency for IFITM3 WT to form aggregates *in vitro* (**Figure EV5A**). Overall, we demonstrate for the first time that IFITM3 is capable of direct interaction with an endosomal Q-SNARE via an R-SNARE-like motif that is critical for antiviral activity.

Since STX7 is an essential part of the SNARE complexes controlling homotypic late endosome fusion and heterotypic late endosome fusion, we determined whether IFITM3 regulates the assembly of the STX7-STX8-Vti1b-VAMP8 complex, the STX7-STX8-Vti1b-VAMP7 complex, or both. STX7, VAMP8, and IFITM3 were ectopically co-expressed in HEK293T and STX7 was immunoprecipitated to identify its interaction partners. As shown above, STX7 pulled down IFITM3 WT, while the G95L mutation in IFITM3 abrogated this interaction (**Figure 5A**). Importantly, STX7 pulled down a reduced amount of VAMP8 in the presence of IFITM3 relative to Empty Vector. In contrast, IFITM3 G95L did not affect the STX7-VAMP8 interaction (**Figure 5A**). These findings were confirmed by measuring the colocalization between STX7-GFP and VAMP8-mCherry in cells expressing IFITM3 WT or IFITM3 G95L. We found that STX7-GFP colocalization with VAMP8-mCherry was reduced by IFITM3 WT in a G95-dependent manner (**Figure 5B**). We performed additional experiments whereby STX7, VAMP7, and IFITM3 were ectopically co-expressed. Here, IFITM3 binding to STX7 did not inhibit the interaction between STX7 and VAMP7. Instead, the STX7-VAMP7 interaction was slightly elevated in the presence of IFITM3 WT, but not IFITM3 G95L (**Figure EV5B**). These results indicate that IFITM3 binding to STX7 selectively impairs the interaction between STX7 and VAMP8.

Since it was previously shown that endocytic viruses including IAV may co-opt the STX7-STX8-Vti1b-VAMP8 SNARE complex to promote the virus entry process (Pirooz *et al.*, 2014b), we performed co-immunoprecipitation experiments in cells that had been inoculated with IAV. Interestingly, we noticed that virus addition resulted in enhanced co-immunoprecipitation between endogenous STX8 and VAMP8 in HEK293T cells (**Figure 5C**).

However, in the presence of ectopic IFITM3 WT, this co-immunoprecipitation was diminished, while co-immunoprecipitation between endogenous STX8 and VAMP7 was enhanced (**Figure 5C**). The IFITM3 G95L mutant, in contrast, co-immunoprecipitated with STX8 to a lesser extent than IFITM3 WT and only marginally impacted the STX8-VAMP8 and STX8-VAMP7 interactions (**Figure 5C**). To address whether endogenous IFITM3 performs a similar function, we immunoprecipitated endogenous STX8 from HeLa. As shown above, endogenous IFITM3 pulls down with endogenous STX8. However, endogenous STX8 pulled down increased quantities of VAMP8 in *IFITM3* KO cells relative to WT cells (**Figure 5D**). Consistently, STX7-GFP colocalized with VAMP8-mCherry to a greater extent in *IFITM3* KO cells compared to WT cells (**Figure EV5C**). These results support a model whereby IFITM3 disfavors the STX7/8-VAMP8 interaction while favoring the STX7/8-VAMP7 interaction. To test whether IFITM3 reduces the assembly of the entire STX7-STX8-Vti1b-VAMP8 SNARE complex involved in homotypic late endosome fusion, we ectopically co-expressed STX7, STX8, Vti1b, and VAMP8 in HEK293T cells. SNARE protein assemblies have been previously characterized as SDS-resistant complexes in whole cell lysates under mildly denaturing conditions (Kubista *et al*, 2004). We identified an SDS-resistant complex approximately 200 kD in size or greater by immunoblotting for VAMP8 (**Figure 6A**) or STX8 (**Appendix Figure S1**). The complex was sensitive to heat, as high molecular weight bands disappeared after boiling lysates (**Figure 6A and Appendix Figure S1**). Consistent with IFITM3 acting as a negative regulator of complex formation, complex abundance was markedly reduced in cells expressing IFITM3 WT (**Figure 6A and Appendix Figure S1**). In contrast, IFITM3 G95L only marginally reduced complex formation (**Figure 6A**). Therefore, by binding STX7/8 via an R-SNARE-like motif and reducing their interaction with VAMP8, IFITM3 impedes formation of the STX7-STX8-Vti1b-VAMP8 complex involved in homotypic late endosome fusion.

Our results showing that IFITM3 uses an R-SNARE-like motif to inhibit assembly of the homotypic late endosome fusion machinery while maintaining, and possibly amplifying, assembly of the heterotypic late endosome-lysosome fusion machinery may explain how IFITM3 redirects incoming virions towards lysosomes for degradation (Feeley *et al.*, 2011; Spence *et al.*, 2018; Suddala *et al.*, 2019). To directly test whether IFITM3 promotes the fusion of late endosomes with lysosomes in living cells, we pulsed cells expressing IFITM3 WT or IFITM3 G95L with Dextran and monitored its trafficking to lysosomes labeled with Magic Red cathepsin substrate. In the presence of IFITM3 WT, Dextran colocalization with lysosomes was enhanced relative to cells expressing Empty Vector or IFITM3 G95L **(Figure 6B)**. When the same assay was performed in HeLa cells, Dextran colocalization with Magic Red was diminished in *IFITM3* KO cells compared to WT cells (**Appendix Figure S1B**). As an alternative approach to measure late endosome-lysosome fusion, we co-transfected cells with Rab7-mCherry and LAMP1-GFP, which label late endosomes and lysosomes, respectively. In cells expressing IFITM3 WT, we observed increased colocalization between Rab7-mCherry and LAMP1-GFP relative to cells expressing Empty Vector or IFITM3 G95L (**Appendix Figure S2**). In contrast, we did not observe extensive colocalization between Rab5-RFP (an early endosome marker) and LAMP1-GFP, and IFITM3 WT did not promote their colocalization (**Appendix Figure S3**). Furthermore, the LAMP1-GFP compartment appeared enlarged and expanded in the presence of IFITM3 WT, which is consistent with enhanced late endosome-lysosome fusion (**Appendix Figures S2 and S3**). While these findings demonstrate that IFITM3 promotes cargo delivery from late endosomes to lysosomes, it remained to be seen whether it promotes endosomal cargo degradation in lysosomes. It was previously reported that IFITM3 accelerates the turnover of the

Epidermal Growth Factor Receptor (EGFR) in lysosomes (Spence *et al.*, 2018). Importantly, the fate of EGFR in cells is also controlled by the STX7-STX8-Vti1b-VAMP7/8 SNARE machinery (Futter *et al*, 1996). To confirm this finding, we took advantage of an assay monitoring the lysosomal turnover of EGFR-GFP by flow cytometry (Inoue *et al*, 2015). We transfected EGFR-GFP into cells expressing Empty Vector, IFITM3 WT, or IFITM3 G95L and treated them with EGF to trigger endocytosis of EGFR-GFP. Under these conditions, a portion of EGFR-GFP is slated for degradation in lysosomes. We found that partial EGFR-GFP loss was detected in HeLa WT cells between 1 and 2 hrs post-EGF addition. In contrast, we did not detect EGFR-GFP loss in HeLa *IFITM3* KO over the same time period (**Appendix Figure S4**). Confirming a role for IFITM3 in accelerating the turnover of EGFR-GFP, we found that EGFR-GFP loss was less marked and less rapid in cells expressing IFITM3 G95L compared to cells expressing IFITM3 WT (**Appendix Figure S4**). Therefore, IFITM3 facilitates the degradation of endosomal cargo by inhibiting assembly of the homotypic late endosome fusion machinery and promoting fusion between late endosomes and lysosomes.

To test the impact of IFITM3 on lysosomal targeting of viral cargo, we examined early steps of IAV entry into cells using confocal immunofluorescence microscopy. In HEK293T cells stably expressing IFITM3 WT or IFITM3 G95L, which differ with respect to STX7 binding potential (**Figure 3A**), IAV was added to cells at a multiplicity of infection of 1 and incubated on ice for 40 mins. Cells were fed warm medium containing Lysotracker, to visualize acidic lysosomes, and placed at 37°C to enable synchronized internalization of virus particles. Four hours later, cells were washed, fixed and immunostained with an antibody against IAV nucleoprotein (NP), which detects incoming, virion-associated NP as well as de novo synthesized NP. In cells expressing Empty Vector, nuclear NP accumulation was apparent at 4 hours post-inoculation in roughly 20% of cells, which signals the initiation of virus replication following successful entry of the virus (i.e. escape from the endocytic compartment) (**Figure 7A and 7B**). In cells expressing IFITM3 WT, nuclear NP accumulation was virtually absent, consistent with strong inhibition of cellular entry of IAV as reported previously (Feeley *et al.*, 2011). In contrast, IFITM3 G95L did not reduce nuclear NP accumulation, in agreement with a loss of antiviral activity exhibited by this mutant (Rahman *et al.*, 2020) (**Figure 7A and 7B**). Interestingly, we observed a negative correlation between the extent of nuclear NP staining and the intensity of Lysotracker staining in cells. IFITM3 WT expression resulted in intensification of Lysotracker fluorescence, consistent with expansion of the lysosomal compartment as described previously (Feeley *et al.*, 2011). However, expression of IFITM3 G95L did not (**Figure 7C and 7D**). In cells expressing IFITM3 G95L, most NP protein localized to the nucleus at four hours post-inoculation. However, some instances of extra-nuclear, bright NP puncta associated with the Lysotracker-positive compartment could be observed, suggesting that a small proportion of incoming IAV virions were trafficked to lysosomes in IFITM3 G95L-expressing cells (**Figure 7D**). However, the occurrence of bright NP puncta colocalizing with Lysotracker-positive vesicles was enhanced in cells expressing IFITM3 WT (**Figure 7D and Appendix Figure S4**). In IFITM3 WT cells, NP was found to colocalize with Lysotracker to a greater extent than in cells expressing IFITM3 G95L (**Figure 7D**). These results support the notion that inhibition of homotypic late endosome fusion and promotion of heterotypic late endosome fusion by IFITM3 underlies its ability to promote trafficking of IAV towards lysosomes (**Figure 8**). Altogether, this body of work demonstrates that endolysosomal SNARE modulation is a key aspect of the mechanism by which IFITM3 protects cells from invading viruses.

Discussion

Our identification of an R-SNARE-like motif in human CD225 proteins suggests that these proteins act as SNARE mimics to regulate SNARE-mediated membrane fusion events. Even though there are CD225 members that lack the polar arginine or glutamine in the central layer characteristic of a canonical SNARE motif, they encode layered hydrophobicity which may still afford some degree of SNARE modulation (**Figure EV1A**). For example, Vti1a is SNARE protein involved in neurotransmission despite encoding an aspartic acid in the central layer (Tang *et al*, 2022) (**Figure 1A**). Moreover, other well-characterized SNARE proteins, like STX8, VAMP8, VAMP7, and Vti1b lack a full complement of hydrophobic layers in their respective SNARE motifs (**Figure 1A**). Since the CD225 family is poorly characterized and contains many proteins with currently unknown functions (Coomer *et al.*, 2021), our discovery of built-in SNARE binding potential within the CD225 domain may serve as a catalyst for uncovering the physiological roles they perform. As such, we provide important insight into the birth and functional expansion of the CD225 domain over the course of evolutionary time.

A limited number of SNARE-like proteins functioning as SNARE mimics have been described before. Two of the best characterized R-SNARE-like proteins in humans are Tomosyn and Amisyn, which adopt VAMP-like protein folds and regulate the same neuronal SNARE complex that PRRT2 does (Hatsuzawa *et al*, 2003; Masuda *et al*, 1998; Scales *et al*, 2002). Furthermore, microbial proteins containing SNARE-like sequence and functionality have been discovered in prokaryotes and viruses (Delevoye *et al*, 2008; King *et al*, 2015; Paumet *et al*, 2009; Shi *et al*, 2016; Wesolowski & Paumet, 2010). Interestingly, phylogenetic evidence suggests that the CD225 domain was introduced into eukaryotes following multiple horizontal transmission events from prokaryotes (Sällman Almén *et al*, 2012). Therefore, it is possible that the SNARE-like motif of CD225 traces its beginnings to a similar, ancient motif in microbes.

IFITM3 was arguably the most completely understood member of the CD225 family, but our finding that it acts as a SNARE assembly modulator significantly boosts our understanding of its key cellular functions. The closely related proteins, IFITM1, IFITM2, IFITM5, and IFITM10, are also likely to interact with SNARE proteins since they all share an R-SNARE-like motif (**Figure 1A**). Interestingly, one of the most significant series of findings with regards to IFITM function was the characterization of a conserved amphipathic alpha helix in its amino terminus. This helix was shown to be essential for the antiviral activity of IFITM3 (Chesarino *et al.*, 2017) and necessary for the ability of IFITM3 to reduce cellular membrane fluidity (Rahman *et al.*, 2020). Following our discovery here, we now know that this amphipathic helix is immediately adjacent to, or part of, an R-SNARE-like motif (**Figure 2A**). Interestingly, a SNARE protein in yeast known as Spo20 also contains an amphipathic alpha helix amino terminal to its SNARE motif, resembling the structural organization of IFITM3 (Nakanishi *et al*, 2004). Moreover, another group of SNARE binding proteins known as complexins are also bestowed with an amphipathic helix, and they use it to induce membrane curvature and stabilize fusion pores produced by SNARE complexes (Courtney *et al*, 2022). Therefore, it is possible that IFITM3 employs its amphipathic helix in conjunction with its R-SNARE-like motif to sculpt membranes at precisely the sites where endolysosomal SNARE assemblies are triggering membrane fusion. Other structural features lend additional support to our case that IFITM3 is a SNARE-like protein. Some SNARE proteins encode a single transmembrane domain to directly anchor into vesicular or target membranes (Jahn & Scheller, 2006), and IFITM3 is similar in this regard (Ling *et al.*, 2016). Additionally, palmitoylation is a post-translational modification of

cysteine residues that promotes membrane localization, and IFITM3 and various SNARE proteins are known to be palmitoylated (Fukasawa *et al*, 2004; Hach *et al.*, 2013; Prekeris *et al*, 2000; Veit *et al*, 1996; Yount *et al*, 2012).

Notably, the relatively limited structural information previously available for IFITM3 did not indicate the presence of a continuous alpha helix reminiscent of a SNARE motif. In isolation, the region comprising the R-SNARE-like sequence motif of IFITM3 was previously thought to form one or two amphipathic helices followed by a disordered, intracellular loop (Chesarino *et al.*, 2017; Ling *et al.*, 2016). The structure of another CD225 protein, PRRT2, was posited to contain a similarly disordered, intracellular loop as well (Rossi *et al*, 2016). The typical SNARE fold characteristic of a SNARE motif may only form in the context of a coiled-coil assembly of multiple SNARE alpha helices (trans-SNARE complex). Our description of IFITM3 as a SNARE-like protein capable of interacting with endosomal SNARE proteins suggests that multiple protein folds and membrane topologies of IFITM3 may be possible, depending on the presence of interacting partners (such as STX7). Thus, attempts to structurally characterize IFITM3 in complex with STX7 or other endosomal SNAREs may provide substantial structural insight that has been lacking.

Regarding the structural interface between IFITM3 and endosomal SNARE proteins, the stoichiometry of the interactions remains unclear. We previously characterized a GxxxG motif present in CD225 proteins that enables homomultimerization and which is essential to the functions of PRRT2 and IFITM3 (Rahman *et al.*, 2020). Here we show that mutation of the GxxxG motif in PRRT2 (G305W), TUSC5 (G141W), or IFITM3 (G95L) caused loss of binding with Q-SNAREs SNAP-25, STX4, or STX7, respectively (**Figure 1B, Figure EV1C and EV1D, and Figure 3A**). These glycines reside adjacent to the +3 hydrophobic layer (**Figure 1A**) and may disrupt the structural integrity of the R-SNARE-like motif. Alternatively, these findings may signal a requirement for CD225 proteins to multimerize prior to gaining SNARE binding potential. Another possibility is that the GxxxG motif in CD225 proteins not only controls homomultimerization but also impacts binding with other proteins including SNAREs.

What is more certain is that this previously unrecognized ability of IFITM3 to bind endosomal SNARE proteins and inhibit homotypic late endosome fusion advances our understanding of how IFITM3 inhibits the cellular entry of a diverse spectrum of enveloped and non-enveloped viruses (Majdoul & Compton, 2021). By showing that IFITM3 inhibits homotypic late endosome fusion while reinforcing heterotypic late endosome fusion, whereby late endosomes fuse with lysosomes, we provide an explanation for how IFITM3 overexpression causes expansion of the endolysosomal compartment and degradation of virions within it (Feeley *et al.*, 2011). Taken together with previous findings, we propose a revised model for the molecular mechanism of IFITM3-mediated antiviral activity that is two-pronged: 1) IFITM3 traps incoming virions in late endosomes by inhibiting membrane fusion between the viral and cellular lipid bilayers; and 2) IFITM3 promotes the fusion of late endosomes with lysosomes to facilitate the degradation of trapped viral cargo.

In addition to blocking infection through inhibition of virus entry into cells, IFITM3 also performs an antiviral function in cells that are already infected—it has been shown to interact with and inhibit the function of viral fusogens (known as viral envelope glycoproteins) found in virions, which in turn reduces the infectivity of said virions (Compton *et al*, 2014; Tartour *et al*, 2014; Wang *et al*, 2017; Yu *et al*, 2015). Remarkably, viral fusogens share structural and functional similarities to SNARE proteins, including heptad repeats and the formation of coiled-coil assemblies to drive membrane merger (Skehel & Wiley, 1998; Sollner, 2004). Therefore, our

description of an R-SNARE-like motif in IFITM3 may reveal the molecular basis by which IFITM3 interacts with both cellular and viral fusion machinery to control virus infections at multiple levels.

Methods

Tissue culture, cell lines, and expression constructs

HEK293T (CRL-3216) and HeLa (CCL-2) were purchased from ATCC and cultivated at 37°C and 5% CO_2 in DMEM (Gibco) complemented with 10% fetal bovine serum (Hyclone) and 1% penicillin-streptomycin (Gibco). HeLa *IFITM3* KO cells were generated as previously described (Shi *et al*, 2018). pQCXIP retroviral vectors encoding human IFITM3 (tagged with FLAG on amino terminus), PRRT2 (tagged with FLAG on carboxy terminus), or TUSC5 (tagged with FLAG on the amino terminus) were previously described (Rahman *et al.*, 2020) or synthesized by Integrated DNA Technologies (IDT) as gBlock fragments and cloned into pQCXIP using BamH1 and EcoR1 restriction enzymes. Mutations were introduced via QuikChange Lightning Site-Directed Mutagenesis (Agilent). HEK293T stably expressing pQCXIP-Empty Vector, pQCXIP-FLAG-IFITM3 WT, or pQCXIP-FLAG-IFITM3 G95L, encoding amino-terminal FLAG tag, were described previously(Rahman *et al.*, 2020). pcDNA3.1 encoding SNARE proteins (SNAP25, STX1A, STX4, STX7, STX8, Vti1b, VAMP8, and VAMP7) tagged with HA or Myc at the amino terminus were synthesized by IDT as gBlock fragments and cloned into pcDNA3.1 using BamH1 and EcoR1 restriction enyzmes. Transfections were performed with Lipofectamine 2000 (Invitrogen). All cell lines tested negative for mycoplasma.

Antibodies, immunoblotting, and immunoprecipitations

Whole cell lysis was performed in a buffer containing 50 mM Tris-HCl pH 7.4, 1.0% TritonX-100 (Sigma), 150 mM NaCl, and 1 mM EDTA. Immunoprecipitation was performed as follows: antibodies were loaded with Dynabeads (Invitrogen) for 1 hr at 4°C while rotating; Dynabead-conjugated antibodies were added to whole cell lysates for 3 hr at 4°C while rotating to capture antibody-antigen complexes; immunoprecipitated fractions were isolated using the DynaMag-2 magnet (Invitrogen) and washed three times with lysis buffer prior to addition of NuPage LDS Sample Buffer (Invitrogen) and NuPage Sample Reducing Agent (Invitrogen); the immunoprecipitated and non-immunoprecipitated fractions were heat denatured at 100°C for 5 min; samples were loaded into Criterion XT 12% Bis-Tris polyacrylamide gels (Bio-Rad) for SDS-PAGE using NuPAGE MES SDS Running Buffer (Invitrogen). Proteins were transferred to Amersham Protran Nitrocellulose Membrane (GE Healthcare), and membranes were blocked with Intercept Blocking Buffer-PBS (Li-COR) prior to incubation with primary and secondary antibodies. The following antibodies were used in this study: anti-STX8 (110-083; Synaptic Systems); anti-STX7 (110-072; Synaptic Systems), anti-Vti1b (164-002; Synaptic Systems), anti-VAMP8 (104-302; Synaptic Systems), anti-VAMP7 (ab36195; Abcam), anti-HA (901514, clone 16B12; Biolegend), anti-HA (ab9110; Abcam (this was used for immunoprecipitation)), anti-Myc (C3956, Sigma), anti-FLAG M2 (F1804; Sigma), anti-IFITM3 (ab109429; Abcam), anti-IFITM2/3 (66081-1-Ig, Proteintech), anti-tubulin (and anti-actin (SC-47778; Santa Cruz Biotechnology). Goat anti-mouse and goat anti-rabbit secondary antibodies conjugated to DyLight 680 or 800 (Li-COR) and the Li-COR Odyssey CLx imaging system were used for generating immunoblots. Membrane images were analyzed using ImageStudioLite (Li-COR).

Sequence retrieval and protein alignments

Protein sequences for CD225 proteins, Q-SNAREs, and R-SNAREs were retrieved from UniProt. Multi-sequence alignments were performed with MEGA11 and manually trimmed to the 53-residue SNARE motif. UniProt numbers for SNAREs are as follows: syntaxin1, Q16623; syntaxin4, Q12846; syntaxin 6, O43752; syntaxin7, O15400; syntaxin8, Q9UNK0; SNAP23, O00161; Vti1a, Q96AJ9; Vti1b, Q9UEU0; VAMP1, P23763; VAMP2, P63027; VAMP3, Q15836; VAMP5, O95183; VAMP7, P51809; VAMP8, Q9BV40; Ykt6, O15498; Syn8p, P31377; Tomosyn/STXBP5, Q5T5C0; Amisyn/STXBP6, Q8NFX7.

Recombinant IFITM3 protein production

Recombinant human IFITM3 protein (WT, F65/68A, and G95L) was produced by cloning the nucleotide sequence appended with a Strep-II tag at the amino terminus into pET3XC and transforming it into Rosetta 2 DE3 pLysS Competent Cells (Sigma). A single colony of transformed cells was grown in LB overnight at 37°C. One mL of the culture was expanded in 200 mL 2YT medium (Sigma) at 37°C until the optical density reached 0.4, and the temperature was lowered to 18°C for 1 hr before induction with 0.4 mM IPTG (Tecknova) for 20 hr. Pelleted cells were frozen at -80°C before proceeding to protein purification. Thawed cells were resuspended in ice cold lysis buffer (at 10% w/v) consisting of 20 mM Tris-HCl pH 7.6, 100 mM NaCl, 1 mM DTT, 0.5 mg/ml lysozyme (Sigma), 1 mM PMSF (Sigma), 0.025% (v/v) Triton X-100 (Sigma), and 1X Complete Protease Inhibitors (Roche). Sample was stirred at 4°C for 20 min before applying 2 freeze-thaw cycles by transferring the sample container between dry ice and a room temperature water bath. The thawed lysate was stirred at room temperature for 15 min after adding 5 U/mL benzonase (Sigma) prior to pulse sonication for 30 s at 4°C. Sample was clarified by centrifugation at 5000 g for 10 min and the supernatant was further centrifuged at 40000 g for 60 min. The pellet was thoroughly resuspended in the lysis buffer (modified to include 1 mM EDTA and excluding lysozyme) and centrifuged at 40000 g for 60 min. This process was then performed a second time. The pellet was extracted twice with 20 mM Tris-HCl pH 7.6, 100 mM NaCl, 20% glycerol, 2% (v/v) Anapoe-X-100 (Anatrace), 1 mM DTT (Gold Bio), and 0.1 mM AEBSF (Santa Cruz Biotechnology) at 4°C while stirring for 4 hr each. The protein in the pellet was extracted with 20 mM Tris-HCl pH 7.6, 0.6% Sarkosyl (w/v) (Sigma), and 2 mM DTT. Strep-II-fused IFITM3 was purified by affinity chromatography using Strep-Tactin Sepharose Resin (IBA Lifesciences). Protein was >90% pure as determined by SDS-PAGE and Coomassie blue staining. Protein concentration was determined by Bio-Rad Protein Assay and stored at a concentration of 15-30 mg/mL at -80°C. In the final reaction mixture of purified, recombinant IFITM3, the Sarkosyl concentration was 0.00002%.

Size exclusion chromatography of recombinant IFITM3

Size exclusion chromatography was performed on a Superose 12 10/300 GL column (GE Healthcare). The column was equilibrated with a buffer consisting of 20 mM Tris-HCl pH 8.0, 120 mM NaCl, 0.2% (v/v) TritonX-100, and 1 mM TCEP. 150 µg recombinant IFITM3 (WT, F75/78A, or G95L) was diluted into 300 µL of buffer and injected into the column. One mL fractions were collected and subjected to SDS-PAGE and Coomassie blue staining.

In vitro protein-protein co-immunoprecipitation

Two µg of recombinant Strep-II tagged IFITM3 WT or F75/78A or G95L were incubated with 2 µg of recombinant His-tagged STX7 (IHUSTX7RN6HISLY50UG; Innovative Research) in 0.3 mL of binding buffer (20 mM HEPES pH 7.4, 150 mM NaCl, 0.2% TritonX-100, and 0.1% BSA) overnight at 4°C. The samples were incubated with 1 µg of anti-STX7 antibody for 1 hr. The antibody-antigen complex was captured with 15 uL of Dynabeads (Invitrogen). After washing the samples 3 times with binding buffer (lacking BSA), proteins captured by beads using the DynaMag-2 were solubilized in 20 uL of 1X NuPAGE LDS Sample Buffer and 1X NuPAGE Sample Reducing Reagent (Invitrogen), and heat denatured at 100°C for 5 min. SDS-PAGE and immunoblotting were performed and proteins were detected as described above.

Structural modeling of the R-SNARE-like motif of IFITM3

The R-SNARE-like motif of IFITM3 (residues 55-113) and the R-SNARE motif of VAMP8 (residues 13-65) were compared by predictive protein structure alignment and comparison algorithm TM-align (Zhang & Skolnick, 2005). A TM score of 0.75847 was recorded, indicating that the two regions are likely to adopt the same alpha helical protein fold. Structural comparison between the R-SNARE-like motif of IFITM3 and the R-SNARE motif of VAMP8, which was previously crystallized as part of the STX7-STX8-Vti1b-VAMP8 trans-SNARE complex (PDB: 1GL2) (Antonin *et al.*, 2002), was performed using Alphafold version 3 (Jumper & Hassabis, 2022) with assistance from the Colabfold server (Mirdita *et al.*, 2022). A structure for the R-SNARE-like motif of IFITM3 was predicted using the R-SNARE motif of VAMP8 as a template. The Alphafold structure was then aligned with that of VAMP8 using the FATCAT server (Li *et al.*, 2020). The aligned structures were then visualized and reoriented for figure presentation using ChimeraX (Meng *et al*, 2023).

Influenza A Virus infection

Influenza A Virus [A/PR/8/34 (PR8), H1N1] supplied as clarified allantoic fluid was purchased from Charles River Laboratories. Infectious virus titers were calculated using a flow cytometry-based method in HEK293T cells (Grigorov *et al*, 2011), and infections were performed as follows: HEK293T cells (transiently transfected with 1.5 µg pQCXIP-Empty Vector, pQCXIP-FLAG-IFITM3 WT, or pQCXIP-FLAG-IFITM3 G95L were seeded in 24-well plates (50,000 per well) overnight and overlaid with virus diluted in 225 µL of complete DMEM (multiplicity of infection = 0.01) for approximately 18 hr. Cells were washed with 1X D-PBS (Gibco), detached with Trypsin-EDTA (Gibco), fixed/permeabilized with Cytofix/Cytoperm (BD), immunostained with anti-IAV NP (ab20343; Abcam), and analyzed on a LSRFortessa flow cytometer (BD).

Influenza A Virus cellular entry assay

An 8-well µ-Slide dish (80826; Ibidi) was coated with 3 mg/mL PureCol (Advanced Biomatrix) for 1 hr at room temperature and then allowed to dry overnight. HEK293T stably expressing pQCXIP-Empty Vector, pQCXIP-FLAG-IFITM3 WT, or pQCXIP-FLAG-IFITM3 G95L were seeded at 20,000 cells per well in DMEM completed with 10% fetal bovine serum and 1% penicillin-streptomycin and incubated at 37°C overnight. Cells were placed on ice for 5 min and then remained on ice while medium was removed and replaced with 120 µL complete DMEM containing Influenza A virus PR8 (multiplicity of infection = 1). Cells mock inoculated with PBS served as a negative control. Inoculated cells were incubated on ice for 40 min to allow for virus adhesion. Medium was removed, cells were washed twice with D-PBS, and medium

was replaced with 150 µL complete DMEM containing 50 nM Lysotracker Deep Red (L12492; Invitrogen) and incubated at 37°C for 4 hr. Medium was removed, cells were washed twice with D-PBS, and cells were fixed/permeabilized with Cytofix/Cytoperm (BD) for 10 min at room temperature. Cells were washed twice with PermWash buffer (BD) and blocked with Intercept Blocking Buffer (PBS) (Li-COR) for 1 hr at room temperature. Cells were immunostained with anti-NP (BE0159; InvivoMab) at a 1:200 dilution in Intercept Antibody Diluent (PBS) (Li-COR) for 1 hr at room temperature. Cells were washed twice in PermWash buffer and goat anti-mouse IgG (H+L) Alexa Fluor 488 secondary antibody (Invitrogen) at 1:300 dilution in Intercept Antibody Diluent (PBS) was added for 1 hr at room temperature. Cells were washed twice in PermWash Buffer and Hoechst 33342 (H3570; Invitrogen) was added for 5 min at room temperature. Cells were washed once in PermWash Buffer and overlaid with 200 µL D-PBS for image acquisition on a Leica Stellaris 5 confocal microscope using the 63X oil objective. Confocal Z stacks of 20-30 optical sections were acquired for each field of view, and multiple fields were imaged per condition. Images were extracted and subjected to analysis in Fiji. To quantify Lysotracker staining, the Corrected Total Cell Fluorescence (CTCF) was measured for the middle Z slice of the entire field. To quantify nuclear NP accumulation, colocalization between NP and Hoechst was measured for the middle Z slick of each cell in the field and a ratio of NP+ nuclei: total nuclei was calculated.

Late endosome-lysosome fusion assay with Dextran pulse-chase and Magic Red labeling

HEK293T cells stably expressing Empty Vector, IFITM3 WT-FLAG, or IFITM3 G95L-FLAG or HeLa cells (WT or *IFITM3* KO) were seeded in 35 mm low µ-Dishes (80136; Ibidi) coated with 3 mg/mL PureCol (Advanced Biomatrix) at 50,000 cells per well in DMEM completed with 10% fetal bovine serum and 1% penicillin-streptomycin and incubated at 37°C overnight. Dextran Alexa Fluor 488 (10,000 MW) (D22910; Invitrogen) was added to cells at a concentration of 25 µg/mL for 2 hrs at 37°C. Dextran-containing medium was then removed, cells were washed three times with D-PBS, fresh DMEM was added, and cells were incubated for 1 hr at 37°C. Cells were washed once with FluoroBrite DMEM (Gibco) completed with 10% fetal bovine serum and 1% penicillin-streptomycin and incubated with Magic Red cathepsin substrate (ab270772; Abcam) (from 250X stock in DMSO, a final concentration of 1X was used) for 5 mins at 37°C. Live cell image acquisition was performed on a Leica Stellaris 5 confocal microscope using the 63X oil objective.

Confocal fluorescence microscopy

HEK293T cells stably expressing pQCXIP-Empty Vector, pQCXIP-FLAG-IFITM3 WT, or pQCXIP-FLAG-IFITM3 G95L or HeLa cells (WT or *IFITM3* KO) were seeded in DMEM completed with 10% fetal bovine serum and 1% penicillin-streptomycin at 500,000 cells per well in a 6-well plate and incubated at 37°C overnight. Cells were transfected with 0.5 µg of the following plasmids: pMRXIP-GFP-STX7 (45921; Addgene), pmCherry-N1-VAMP8 (92424; Addgene), pEGFP-N3-LAMP1 (34831; Addgene), pmRFP-C3-Rab5 (14437; Addgene), or pmCherry-Rab7a-7 (55127; Addgene) using Lipofectamine 2000 (Invitrogen). Medium was replaced 6 hrs post-transfection, and cells were incubated at 37°C for 18 hrs. Cells were washed once with D-PBS and fixed with Cytofix/Cytoperm (BD). For immunofluorescence analysis of IFITM3 expression, immunostaining was performed with anti-FLAG M2 (F1804; Sigma) in fixed cells.

EGFR-GFP degradation assay

HEK293T cells stably expressing pQCXIP-Empty Vector, pQCXIP-FLAG-IFITM3 WT, or pQCXIP-FLAG-IFITM3 G95L or HeLa cells (WT or *IFITM3* KO) were seeded in DMEM completed with 10% fetal bovine serum and 1% penicillin-streptomycin at 500,000 cells per well in a 6-well plate and incubated at 37°C overnight. Cells were transfected with 0.5 µg of EGFR-GFP using Lipofectamine 2000. Medium was replaced 6 hrs post-transfection, and cells were incubated at 37°C for 18 hrs. Recombinant EGF (R&D Systems) was added to cells and, at the indicate time point, cells were washed once with D-PBS and fixed with Cytofix/Cytoperm (BD). The percentage of EGFR-GFP+ cells was measured by flow cytometry on an LSRFortessa (BD).

Statistics

Statistical differences were determined with one-way ANOVA test or student's t test corrected for multiple comparisons, using an alpha cut-off of 0.05. All tests were performed as two-tailed and unpaired. Test type and *P* values are reported in the figure captions.

Data deposition and availability

This study includes no data deposited in external repositories. All data are available in the Source Data files.

Acknowledgements

We would like to thank Alexis Schirling for assisting in molecular cloning of SNARE proteins and Guoli Shi for assisting with confocal immunofluorescence microscopy. This work was supported by funding from the Intramural Research Program, National Institutes of Health.

Disclosure and Competing Interests Statement

The authors declare no competing interests.

References

Advani RJ, Yang B, Prekeris R, Lee KC, Klumperman J, Scheller RH (1999) VAMP-7 mediates vesicular transport from endosomes to lysosomes. *J Cell Biol* 146: 765-776

Antonin W, Fasshauer D, Becker S, Jahn R, Schneider TR (2002) Crystal structure of the endosomal SNARE complex reveals common structural principles of all SNAREs. *Nat Struct Biol* 9: 107-111

Bailey CC, Huang IC, Kam C, Farzan M (2012) Ifitm3 limits the severity of acute influenza in mice. *PLoS Pathogens* 8: e1002909

Beaton N, Rudigier C, Moest H, Müller S, Mrosek N, Röder E, Rudofsky G, Rülicke T, Ukropec J, Ukropcova B *et al* (2015) TUSC5 regulates insulin-mediated adipose tissue glucose uptake by modulation of GLUT4 recycling. *MOLMET* 4: 795-810

Becker F, Schubert J, Striano P, Anttonen AK, Liukkonen E, Gaily E, Gerloff C, Muller S, Heussinger N, Kellinghaus C *et al* (2013) PRRT2-related disorders: further PKD and ICCA cases and review of the literature. *J Neurol* 260: 1234-1244

Chesarino NM, Compton AA, McMichael TM, Kenney AD, Zhang L, Soewarna V, Davis M, Schwartz O, Yount JS (2017) IFITM3 requires an amphipathic helix for antiviral activity. *EMBO Reports* 18: e201744100-201744112

Chesarino NM, McMichael TM, Yount JS (2014) Regulation of the trafficking and antiviral activity of IFITM3 by post-translational modifications. *Future Microbiology* 9: 1151-1163

Coleman J, Jouannot O, Ramakrishnan SK, Zanetti MN, Wang J, Salpietro V, Houlden H, Rothman JE, Krishnakumar SS (2018) PRRT2 Regulates Synaptic Fusion by Directly Modulating SNARE Complex Assembly. *Cell Reports* 22: 820-831

Compton AA, Bruel T, Porrot F, Mallet A, Sachse M, Euvrard M, Liang C, Casartelli N, Schwartz O (2014) IFITM Proteins Incorporated into HIV-1 Virions Impair Viral Fusion and Spread. *Cell Host Microbe* 16: 736-747

Compton AA, Roy N, Porrot F, Billet A, Casartelli N, Yount JS, Liang C, Schwartz O (2016) Natural mutations in IFITM3 modulate post-translational regulation and toggle antiviral specificity. *EMBO Reports* 17: 1657-1671

Coomer CA, Rahman K, Compton AA (2021) CD225 Proteins: A Family Portrait of Fusion Regulators. *Trends in Genetics* 7: 1-4

Courtney KC, Wu L, Mandal T, Swift M, Zhang Z, Alaghemandi M, Wu Z, Bradberry MM, Deo C, Lavis LD *et al* (2022) The complexin C-terminal amphipathic helix stabilizes the fusion pore open state by sculpting membranes. *Nat Struct Mol Biol* 29: 97-107

Delevoye C, Nilges M, Dehoux P, Paumet F, Perrinet S, Dautry-Varsat A, Subtil A (2008) SNARE protein mimicry by an intracellular bacterium. *PLoS Pathogens* 4: e1000022

Desai TM, Marin M, Chin CR, Savidis G, Brass AL, Melikyan GB (2014) IFITM3 restricts influenza A virus entry by blocking the formation of fusion pores following virus-endosome hemifusion. *PLoS Pathogens* 10: e1004048

Ebrahimi-Fakhari D, Saffari A, Westenberger A, Klein C (2015) The evolving spectrum of PRRT2-associated paroxysmal diseases. *Brain* 138: 3476-3495

Everitt AR, Clare S, Pertel T, John SP, Wash RS, Smith SE, Chin CR, Feeley EM, Sims JS, Adams DJ *et al* (2012) IFITM3 restricts the morbidity and mortality associated with influenza. *Nature* 484: 519-523

Fasshauer D, Sutton RB, Brunger AT, Jahn R (1998) Conserved structural features of the synaptic fusion complex: SNARE proteins reclassified as Q- and R-SNAREs. *Proc Natl Acad Sci U S A* 95: 15781-15786

Fazakerley DJ, Naghiloo S, Chaudhuri R, Koumanov F, Burchfield JG, Thomas KC, Krycer JR, Prior MJ, Parker BL, Murrow BA *et al* (2015) Proteomic Analysis of GLUT4 Storage Vesicles Reveals Tumor Suppressor Candidate 5 (TUSC5) as a Novel Regulator of Insulin Action in Adipocytes. *J Biol Chem* 290: 23528-23542

Feeley EM, Sims JS, John SP, Chin CR, Pertel T, Chen L-M, Gaiha GD, Ryan BJ, Donis RO, Elledge SJ *et al* (2011) IFITM3 inhibits influenza A virus infection by preventing cytosolic entry. *PLoS Pathogens* 7: e1002337

Fukasawa M, Varlamov O, Eng WS, Sollner TH, Rothman JE (2004) Localization and activity of the SNARE Ykt6 determined by its regulatory domain and palmitoylation. *Proc Natl Acad Sci U S A* 101: 4815-4820

Futter CE, Pearse A, Hewlett LJ, Hopkins CR (1996) Multivesicular endosomes containing internalized EGF-EGF receptor complexes mature and then fuse directly with lysosomes. *J Cell Biol* 132: 1011-1023

Grigorov B, Rabilloud J, Lawrence P, Gerlier D (2011) Rapid Titration of Measles and Other Viruses: Optimization with Determination of Replication Cycle Length. *PLoS ONE* 6: e24135-24112

Guo X, Steinkühler J, Marin M, Li X, Lu W, Dimova R, Melikyan GB (2021) Interferon-Induced Transmembrane Protein 3 Blocks Fusion of Diverse Enveloped Viruses by Altering Mechanical Properties of Cell Membranes. *ACS Nano* 15(5): 8155-8170

Hach JC, McMichael T, Chesarino NM, Yount JS (2013) Palmitoylation on Conserved and Nonconserved Cysteines of Murine IFITM1 Regulates Its Stability and Anti-Influenza A Virus Activity. *Journal of Virology* 87: 9923-9927

Han J, Pluhackova K, Bockmann RA (2017) The Multifaceted Role of SNARE Proteins in Membrane Fusion. *Front Physiol* 8: 5

Hatsuzawa K, Lang T, Fasshauer D, Bruns D, Jahn R (2003) The R-SNARE motif of tomosyn forms SNARE core complexes with syntaxin 1 and SNAP-25 and down-regulates exocytosis. *J Biol Chem* 278: 31159-31166

Hong W (2005) SNAREs and traffic. *Biochim Biophys Acta* 1744: 493-517

Inoue H, Matsuzaki Y, Tanaka A, Hosoi K, Ichimura K, Arasaki K, Wakana Y, Asano K, Tanaka M, Okuzaki D *et al* (2015) γ-SNAP stimulates disassembly of endosomal SNARE complexes and regulates endocytic trafficking pathways. *J Cell Sci* 128: 2781-2794

Jahn R, Scheller RH (2006) SNAREs — engines for membrane fusion. *Nat Rev Mol Cell Bio* 7: 631-643

John SP, Chin CR, Perreira JM, Feeley EM, Aker AM, Savidis G, Smith SE, Elia AEH, Everitt AR, Vora M *et al* (2013) The CD225 domain of IFITM3 is required for both IFITM protein association and inhibition of influenza A virus and dengue virus replication. *Journal of Virology* 87: 7837-7852

Jumper J, Hassabis D (2022) Protein structure predictions to atomic accuracy with AlphaFold. *Nat Methods* 19: 11-12

King NP, Newton P, Schuelein R, Brown DL, Petru M, Zarsky V, Dolezal P, Luo L, Bugarcic A, Stanley AC *et al* (2015) Soluble NSF attachment protein receptor molecular mimicry by a Legionella pneumophila Dot/Icm effector. *Cell Microbiol* 17: 767-784

Klein S, Golani G, Lolicato F, Lahr C, Beyer D, Herrmann A, Wachsmuth-Melm M, Reddmann N, Brecht R, Hosseinzadeh M *et al* (2023) IFITM3 blocks influenza virus entry by sorting lipids and stabilizing hemifusion. *Cell Host Microbe* 31: 616-633 e620

Kloepper TH, Kienle CN, Fasshauer D (2007) An elaborate classification of SNARE proteins sheds light on the conservation of the eukaryotic endomembrane system. *Mol Biol Cell* 18: 3463-3471

Kubista H, Edelbauer H, Boehm S (2004) Evidence for structural and functional diversity among SDS-resistant SNARE complexes in neuroendocrine cells. *J Cell Sci* 117: 955-966

Li C, Guo XR, Dong ZM, Gao YJ, Li XL, Zhang L, Zheng HQ, Wang LL, Lu C, Tian XX *et al* (2024) Novel interacting proteins identified by tandem affinity purification and mass spectrometry associated with IFITM3 protein during PDCoV infection. *Int J Biol Macromol* 277: 132755

Li K, Markosyan RM, Zheng Y-M, Golfetto O, Bungart B, Li M, Ding S, He Y, Liang C, Lee JC *et al* (2013) IFITM proteins restrict viral membrane hemifusion. *PLoS Pathogens* 9: e1003124

Li Z, Jaroszewski L, Iyer M, Sedova M, Godzik A (2020) FATCAT 2.0: towards a better understanding of the structural diversity of proteins. *Nucleic Acids Res* 48: W60-W64

Ling S, Zhang C, Wang W, Cai X, Yu L, Wu F, Zhang L, Tian C (2016) Combined approaches of EPR and NMR illustrate only one transmembrane helix in the human IFITM3. *Scientific Reports* 6: 1-8

Ma H, Feng S, Deng X, Wang L, Zeng S, Wang C, Ma X, Sun H, Chen R, Du S *et al* (2018) A PRRT2 variant in a Chinese family with paroxysmal kinesigenic dyskinesia and benign familial infantile seizures results in loss of interaction with STX1B. *Epilepsia* 59: 1621-1630

Majdoul S, Compton AA (2021) Lessons in self-defence: inhibition of virus entry by intrinsic immunity. *Nat Rev Immunol* 22(6): 339-352

Masuda ES, Huang BC, Fisher JM, Luo Y, Scheller RH (1998) Tomosyn binds t-SNARE proteins via a VAMP-like coiled coil. *Neuron* 21: 479-480

Meng EC, Goddard TD, Pettersen EF, Couch GS, Pearson ZJ, Morris JH, Ferrin TE (2023) UCSF ChimeraX: Tools for structure building and analysis. *Protein Sci* 32: e4792

Mirdita M, Schutze K, Moriwaki Y, Heo L, Ovchinnikov S, Steinegger M (2022) ColabFold: making protein folding accessible to all. *Nat Methods* 19: 679-682

Mullock BM, Smith CW, Ihrke G, Bright NA, Lindsay M, Parkinson EJ, Brooks DA, Parton RG, James DE, Luzio JP *et al* (2000) Syntaxin 7 is localized to late endosome compartments, associates with Vamp 8, and Is required for late endosome-lysosome fusion. *Mol Biol Cell* 11: 3137-3153

Nakanishi H, de los Santos P, Neiman AM (2004) Positive and negative regulation of a SNARE protein by control of intracellular localization. *Mol Biol Cell* 15: 1802-1815

Paumet F, Wesolowski J, Garcia-Diaz A, Delevoye C, Aulner N, Shuman HA, Subtil A, Rothman JE (2009) Intracellular Bacteria Encode Inhibitory SNARE-Like Proteins. *PLoS ONE* 4: e7375-7379

Pirooz S, He S, O'Connell D, Khalilzadeh P, Yang Y, Liang C (2014a) Viruses customize autophagy protein for efficient viral entry. *Autophagy* 10: 1355-1356

Pirooz SD, He S, Zhang T, Zhang X, Zhao Z, Oh S, O'Connell D, Khalilzadeh P, Amini-Bavil-Olyaee S, Farzan M *et al* (2014b) UVRAG is required for virus entry through combinatorial interaction with the class C-Vps complex and SNAREs. *Proc Natl Acad Sci U S A* 111: 2716-2721

Prekeris R, Klumperman J, Scheller RH (2000) Syntaxin 11 is an atypical SNARE abundant in the immune system. *Eur J Cell Biol* 79: 771-780

Prekeris R, Yang B, Oorschot V, Klumperman J, Scheller RH (1999) Differential roles of syntaxin 7 and syntaxin 8 in endosomal trafficking. *Mol Biol Cell* 10: 3891-3908

Pryor PR, Mullock BM, Bright NA, Lindsay MR, Gray SR, Richardson SCW, Stewart A, James DE, Piper RC, Luzio JP (2004) Combinatorial SNARE complexes with VAMP7 or VAMP8 define different late endocytic fusion events. *EMBO Reports* 5: 590-595

Rahman K, Coomer CA, Majdoul S, Ding SY, Padilla-Parra S, Compton AA (2020) Homology-guided identification of a conserved motif linking the antiviral functions of IFITM3 to its oligomeric state. *eLife* 9: 975-925

Rahman K, Datta SAK, Beaven AH, Jolley AA, Sodt AJ, Compton AA (2022) Cholesterol Binds the Amphipathic Helix of IFITM3 and Regulates Antiviral Activity. *J Mol Biol* 434: 167759

Rossi P, Sterlini B, Castroflorio E, Marte A, Onofri F, Valtorta F, Maragliano L, Corradi A, Benfenati F (2016) A Novel Topology of Proline-rich Transmembrane Protein 2 (PRRT2). *J Biol Chem* 291: 6111-6123

Sällman Almén M, Bringeland N, Fredriksson R, Schiöth HB (2012) The Dispanins: A Novel Gene Family of Ancient Origin That Contains 14 Human Members. *PLoS ONE* 7: e31961

Scales SJ, Hesser BA, Masuda ES, Scheller RH (2002) Amisyn, a novel syntaxin-binding protein that may regulate SNARE complex assembly. *J Biol Chem* 277: 28271-28279

Shi G, Ozog S, Torbett BE, Compton AA (2018) mTOR inhibitors lower an intrinsic barrier to virus infection mediated by IFITM3. *Proc Natl Acad Sci U S A* 115: E10069-E10078

Shi G, Schwartz O, Compton AA (2017) More than meets the I: the diverse antiviral and cellular functions of interferon-induced transmembrane proteins. *Retrovirology* 14: 1-11

Shi X, Halder P, Yavuz H, Jahn R, Shuman HA (2016) Direct targeting of membrane fusion by SNARE mimicry: Convergent evolution of Legionella effectors. *Proc Natl Acad Sci U S A* 113: 8807-8812

Skehel JJ, Wiley DC (1998) Coiled coils in both intracellular vesicle and viral membrane fusion. *Cell* 95: 871-874

Sollner TH (2004) Intracellular and viral membrane fusion: a uniting mechanism. *Curr Opin Cell Biol* 16: 429-435

Spence JS, He R, Hoffmann H-H, Das T, Thinon E, Rice CM, Peng T, Chandran K, Hang HC (2018) IFITM3 directly engages and shuttles incoming virus particles to lysosomes. *Nat Chem Biol* 1: 1-15

St-Denis JF, Cushman SW (1998) Role of SNARE's in the GLUT4 translocation response to insulin in adipose cells and muscle. *J Basic Clin Physiol Pharmacol* 9: 153-165

Stöckli J, Fazakerley DJ, James DE (2011) GLUT4 exocytosis. *J Cell Sci* 124: 4147-4159

Suddala KC, Lee CC, Meraner P, Marin M, Markosyan RM, Desai TM, Cohen FS, Brass AL, Melikyan GB (2019) Interferon-induced transmembrane protein 3 blocks fusion of sensitive but not resistant viruses by partitioning into virus-carrying endosomes. *PLoS Pathogens* 15: e1007532-1007535

Sudhof TC (2004) The synaptic vesicle cycle. *Annu Rev Neurosci* 27: 509-547

Sutton RB, Fasshauer D, Jahn R, Brunger AT (1998) Crystal structure of a SNARE complex involved in synaptic exocytosis at 2.4 A resolution. *Nature* 395: 347-353

Tan GH, Liu YY, Wang L, Li K, Zhang ZQ, Li HF, Yang ZF, Li Y, Li D, Wu MY *et al* (2018) PRRT2 deficiency induces paroxysmal kinesigenic dyskinesia by regulating synaptic transmission in cerebellum. *Cell Res* 28: 90-110

Tang F, Fan J, Zhang X, Zou Z, Xiao D, Li X (2022) The Role of Vti1a in Biological Functions and Its Possible Role in Nervous System Disorders. *Front Mol Neurosci* 15: 918664

Tartour K, Appourchaux R, Gaillard J, Nguyen X-N, Durand Sp, Turpin J, Beaumont E, Roch E, Berger G, Mahieux R *et al* (2014) IFITM proteins are incorporated onto HIV-1 virion particles and negatively imprint their infectivity. *Retrovirology* 11: 103

Valente P, Castroflorio E, Rossi P, Fadda M, Sterlini B, Cervigni RI, Prestigio C, Giovedì S, Onofri F, Mura E *et al* (2016) PRRT2 Is a Key Component of the Ca2+-Dependent Neurotransmitter Release Machinery. *Cell Reports* 15: 117-131

Varadi M, Bertoni D, Magana P, Paramval U, Pidruchna I, Radhakrishnan M, Tsenkov M, Nair S, Mirdita M, Yeo J *et al* (2024) AlphaFold Protein Structure Database in 2024: providing structure coverage for over 214 million protein sequences. *Nucleic Acids Res* 52: D368-D375

Veit M, Sollner TH, Rothman JE (1996) Multiple palmitoylation of synaptotagmin and the t-SNARE SNAP-25. *FEBS Lett* 385: 119-123

Wang Y, Pan Q, Ding S, Wang Z, Yu J, Finzi A, Liu S-L, Liang C (2017) The V3 Loop of HIV-1 Env Determines Viral Susceptibility to IFITM3 Impairment of Viral Infectivity. *Journal of Virology* 91: e02441-02416-02417

Wesolowski J, Paumet F (2010) SNARE motif: a common motif used by pathogens to manipulate membrane fusion. *Virulence* 1: 319-324

Wojnacki J, Nola S, Bun P, Cholley B, Filippini F, Presse MT, Lipecka J, Lam SM, N'Guyen J, Simon A *et al* (2021) Role of VAMP7-dependent secretion of reticulon 3 in neurite growth. *Cell Reports* 35: 109006

Xiao W, Poirier MA, Bennett MK, Shin YK (2001) The neuronal t-SNARE complex is a parallel four-helix bundle. *Nat Struct Biol* 8: 308-311

Yount JS, Karssemeijer RA, Hang HC (2012) S-palmitoylation and ubiquitination differentially regulate interferon-induced transmembrane protein 3 (IFITM3)-mediated resistance to influenza virus. *J Biol Chem* 287: 19631-19641

Yount JS, Moltedo B, Yang Y-Y, Charron G, Moran TM, López CB, Hang HC (2010) Palmitoylome profiling reveals S-palmitoylation-dependent antiviral activity of IFITM3. *Nat Chem Biol* 6: 610-614

Yu J, Li M, Wilkins J, Ding S, Swartz TH, Esposito AM, Zheng Y-M, Freed EO, Liang C, Chen BK *et al* (2015) IFITM Proteins Restrict HIV-1 Infection by Antagonizing the Envelope Glycoprotein. *Cell Reports* 13: 1-13

Zhang Y, Skolnick J (2005) TM-align: a protein structure alignment algorithm based on the TM-score. *Nucleic Acids Res* 33: 2302-2309

Figure Legends

Figure 1: CD225 proteins contain a motif resembling an R-SNARE motif.
(A) A selection of SNARE proteins from yeast and mammals were aligned with proteins with SNARE-like motifs, and a 53-residue stretch of sequence is shown. Proteins are grouped by Q-SNARE, R-SNARE, or R-SNARE-like, and CD225 proteins are labeled as a subset of the R-SNARE-like proteins. Residues in red text are the central polar arginine or glutamine residues characteristic of canonical SNARE proteins and are labeled as the central “0” layer. Surrounding heptad repeats of hydrophobic residues are labeled from “-7” to “+8” in relation to the “0” layer, and sites highlighted in yellow correspond to hydrophobic residues. Underlined residues are those found in PRRT2, which when mutated, are associated with neurological dysfunction. (B) Left: HEK293T cells were co-transfected with SNAP25-HA and either PRRT2-FLAG (WT, R295Q, G305W, or A320V) or Empty Vector. SDS-PAGE and immunoblotting were performed with anti-HA and anti-FLAG in whole cell lysates. Anti-actin was used as loading control. Right: From co-transfected cells, SNAP25-HA was immunoprecipitated with anti-HA followed by SDS-PAGE and immunoblotting with anti-HA and anti-FLAG. Immunoglobulin chain was used as loading control. Numbers and tick marks left of blots indicate position and size (in kilodaltons) of protein standard in ladder. The FLAG/HA ratio was calculated for the indicated lanes and shown as mean and standard error (normalized relative to WT, which was set to 100%). Differences that were statistically significant from WT as determined by one-way ANOVA are indicated by (*). Exact p values are as follows (from left to right): $p < 0.0001$, $p < 0.0001$, $p < 0.0001$. Immunoblots were performed independently three times (biological replicates), and a representative example is shown. Sc; Saccharomyces cerevisiae. Ig; immunoglobulin. IP; immunoprecipitation. EV; empty vector. WT; wild-type.

Figure 2: IFITM3 contains an R-SNARE-like motif and interacts with ectopic endosomal Q-SNARE STX7.
(A) Human endosomal SNARE proteins were aligned with aligned with human IFITM proteins, and a 53-residue stretch of sequence is shown. Residues in red text are the central polar arginine

or glutamine residues characteristic of canonical SNARE proteins and are labeled as the central "0" layer. Surrounding heptad repeats of hydrophobic residues are labeled from "-7" to "+8" in relation to the "0" layer, and sites highlighted in yellow correspond to hydrophobic residues. Black underlined residues in IFITM3 which were mutated for functional experiments. Green underlined residues in IFITM3 correspond to the previously described amphipathic alpha helix. (B) HEK293T cells were transfected with IFITM3-FLAG (WT, F75/78A, R85Q, or G95L) and, 48 hours later, challenged with IAV (A/PR/8/34 (PR8), H1N1) at a multiplicity of infection of 0.10. 18 hours post-infection, cells were fixed, permeabilized, immunostained with anti-FLAG and anti-NP, and analyzed by flow cytometry. The percentage of NP+ cells was measured as a fraction of FLAG+ cells and shown as mean and standard error (normalized relative to Empty Vector, which was set to 100%). Infections were performed independently three times (biological replicates). Differences that were statistically significant from WT as determined by one-way ANOVA are indicated by (*). Exact p values are as follows (from left to right): $p < 0.0001$, $p < 0.0001$, $p < 0.0001$. (C) Structural prediction of the R-SNARE-like motif of IFITM3 was performed with Alphafold and FATCAT. Residues 55-113 of IFITM3 were modeled against a template of the R-SNARE motif of VAMP8 which was previously crystallized as part of the STX7-STX8-Vti1b-VAMP8 trans-SNARE complex (PDB: 1GL2). (D) Left: HEK293T cells were co-transfected with IFITM3-FLAG or Empty Vector and a construct encoding a single SNARE protein: STX7-HA, STX8-HA, Vti1b-HA, VAMP8-HA, or VAMP7-myc. SDS-PAGE and immunoblotting were performed with anti-HA, anti-myc, and anti-FLAG in whole cell lysates. Anti-actin was used as loading control. Right: From co-transfected cells, IFITM3-FLAG was immunoprecipitated with anti-FLAG followed by SDS-PAGE and immunoblotting with anti-HA, anti-myc, and anti-FLAG. Heavy chain immunoglobulin chain was used as loading control. Co-transfection of Empty Vector and STX7-HA was used as a negative control for immunoprecipitation. (E) Left: HEK293T cells were co-transfected with STX7-HA and either IFITM3-FLAG (WT, F75/78A, or R85Q) or Empty Vector. SDS-PAGE and immunoblotting were performed with anti-HA and anti-FLAG in whole cell lysates. Anti-actin was used as loading control. Right: From co-transfected cells, IFITM3-FLAG was immunoprecipitated with anti-FLAG followed by SDS-PAGE and immunoblotting with anti-FLAG and anti-HA. Light chain immunoglobulin was used as loading control. Co-transfection of Empty Vector and STX7-HA was used as a negative control for immunoprecipitation. The HA/FLAG ratio was calculated for the indicated lanes and shown as mean and standard error (normalized relative to WT, which was set to 100%). Differences that were statistically significant from WT as determined by one-way ANOVA are indicated by (*). Exact p values are as follows (from left to right): $p < 0.0001$, $p < 0.0001$. Numbers and tick marks left of blots indicate position and size (in kilodaltons) of protein standard in ladder. Immunoblots were performed independently three times, and a representative example is shown. IAV; Influenza A virus. Ig; immunoglobulin. IP; immunoprecipitation. EV; Empty Vector. WT; wild-type.

Figure 3: IFITM3 interacts with endosomal Q-SNAREs in a G95-dependent manner

(A) Top: HEK293T cells were co-transfected with STX8-HA, STX7-HA, or Vti1b-HA and either Empty Vector or IFITM3-FLAG (WT, F75/78A, or G95L). SDS-PAGE and immunoblotting were performed with anti-HA and anti-FLAG in whole cell lysates. Anti-tubulin was used as loading control. Bottom: from co-transfected cells, STX8-HA, STX7-HA, or Vti1b-HA were immunoprecipitated with anti-HA followed by SDS-PAGE and immunoblotting with anti-HA and anti-FLAG. Heavy chain immunoglobulin was used as loading control. Co-transfection of

Empty Vector and STX8-HA was used as a negative control for immunoprecipitation. The FLAG/HA ratio was calculated for the indicated lanes and shown as mean and standard error (normalized relative to WT with STX7-HA, which was set to 100%). Differences that were statistically significant from WT with STX7-HA as determined by one-way ANOVA are indicated by (*). Exact *p* values are as follows (from left to right): $p < 0.0001$, $p < 0.0001$, $p < 0.0001$, $p < 0.0001$, $p < 0.0001$. Numbers and tick marks left of blots indicate position and size (in kilodaltons) of protein standard in ladder. Immunoblots were performed independently three times, and a representative example is shown. (B) HEK293T cells stably expressing Empty Vector, IFITM3 WT-FLAG, or IFITM3 G95L-FLAG were transfected with STX7-GFP, fixed, immunostained with anti-FLAG, and analyzed by confocal immunofluorescence microscopy. Colocalization was measured between FLAG and STX7-GFP by calculating the Pearson's Correlation Coefficient using Fiji software. Coefficients were calculated from medial Z-slices from three fields of view containing 5-15 cells per condition and presented as means and standard error. Scale bar = 15 microns. Ig; immunoglobulin. IP; immunoprecipitation. EV; Empty Vector. WT; wild-type. PCC; Pearson's Correlation Coefficient.

Figure 4: Endogenous IFITM3 interacts with endosomal Q-SNAREs and R-SNAREs via an R-SNARE-like motif.

(A) Left: HeLa cells (WT or *IFITM3* KO) were transfected with STX7-HA. SDS-PAGE and immunoblotting were performed with anti-HA and anti-IFITM3 in whole cell lysates. Anti-actin was used as loading control. Right: STX7-HA was immunoprecipitated with anti-HA antibody followed by SDS-PAGE and immunoblotting with anti-HA and anti-IFITM3. Heavy chain immunoglobulin was used as loading control. An isotype matched antibody was used as a control for immunoprecipitation. (B) Endogenous STX8 was immunoprecipitated from HeLa (WT or *IFITM3* KO) with anti-STX8 followed by SDS-PAGE and immunoblotting with anti-STX8 and anti-IFITM3. Heavy chain immunoglobulin was used as loading control. An isotype matched antibody was used as a control for immunoprecipitation. The (#) symbol denotes the presence of light chain immunoglobulin. (C) Endogenous Vti1b was immunoprecipitated from HeLa (WT or *IFITM3* KO) with anti-Vti1b followed by SDS-PAGE and immunoblotting with anti-Vti1b and anti-IFITM3. Light chain immunoglobulin was used as loading control. (D) Endogenous VAMP8 was immunoprecipitated from HeLa (WT or *IFITM3* KO) with anti-VAMP8 followed by SDS-PAGE and immunoblotting with anti-VAMP8 and anti- IFITM3. Light chain immunoglobulin was used as loading control. (E) Endogenous VAMP7 was immunoprecipitated from HeLa (WT or *IFITM3* KO) with anti-VAMP7 followed by SDS-PAGE and immunoblotting with anti-VAMP7 and anti-IFITM3. Two forms of VAMP7 were detected following immunoprecipitation: one form of approximately 25 kD and another of approximately 15 kD (Wojnacki *et al*, 2021). Light chain immunoglobulin was used as loading control. (F) Left: Recombinant STX7 and recombinant IFITM3 (WT, F75/78A, or G95L) were mixed together in vitro and reaction inputs were visualized by SDS-PAGE and immunoblotting with anti-STX7 and anti-IFITM3. Right: recombinant STX7 was immunoprecipitated with anti-STX7 followed by SDS-PAGE and immunoblotting with anti-STX7 and anti-IFITM3. Heavy chain immunoglobulin was used as loading control. Numbers and tick marks left of blots indicate position and size (in kilodaltons) of protein standard in ladder. Immunoblots were performed independently two times and a representative example is shown. Ig; immunoglobulin. IP; immunoprecipitation. KO; knockout. WT; wild-type. r; recombinant.

Figure 5: IFITM3 inhibits the interaction between STX7/8 and VAMP8. (A) HEK293T cells stably expressing Empty Vector, IFITM3 WT-FLAG, or IFITM3 G95L-FLAG were co-transfected with STX7-HA and VAMP8-Myc. Whole cell lysates were subjected to SDS-PAGE and immunoblotting with anti-HA, anti-FLAG, and anti-Myc. Actin was used as a loading control. Right: STX7-HA was immunoprecipitated with anti-HA followed by SDS-PAGE and immunoblotting with anti-HA, anti-FLAG, and anti-Myc. The Myc/HA ratio was calculated for the indicated lanes and shown as mean and standard error (normalized relative to Empty Vector, which was set to 100%). Differences that were statistically significant from Empty Vector as determined by one-way ANOVA are indicated by (*). Exact *p* values are as follows (from left to right): $p = 0.0016$, $p = 0.4318$. (B) HEK293T cells stably expressing Empty Vector, IFITM3 WT-FLAG, or IFITM3 G95L-FLAG were transfected with STX7-GFP and VAMP8-mCherry, fixed, and analyzed by confocal immunofluorescence microscopy. Colocalization was measured between STX7-GFP and VAMP8-mCherry by calculating the Pearson's Correlation Coefficient using Fiji software. Coefficients were calculated from medial Z-slices from three fields of view containing 5-15 cells per condition and presented as means and standard error. Scale bar = 15 microns. (C) HEK293T cells stably expressing Empty Vector, IFITM3 WT-FLAG, or IFITM3 G95L-FLAG were inoculated with IAV (+) or medium (-) for 18 hours and subjected to whole cell lysis. Endogenous STX8 was immunoprecipitated with anti-STX8 followed by SDS-PAGE and immunoblotting with anti-STX8, anti-FLAG, anti-VAMP8, and anti-VAMP7. The VAMP8/STX8 and VAMP7/STX8 ratios were calculated for the indicated lanes and shown as mean and standard error (normalized relative to No Virus Empty Vector, which was set to 100%). Differences that were statistically significant from No Virus Empty Vector as determined by one-way ANOVA are indicated by (*). Exact *p* values are as follows (from left to right, top to bottom): $p = 0.0007$, $p = 0.6986$, $p = 0.0093$, $p = 0.4523$, $p < 0.0001$, $p = 0.7960$. (D) Endogenous STX8 was immunoprecipitated from HeLa cells (WT or *IFITM3* KO) with anti-STX8 followed by SDS-PAGE and immunoblotting with anti-STX8, anti-IFITM3, and anti-VAMP8. Light chain immunoglobulin was used as loading control. An isotype matched antibody was used as a control for immunoprecipitation. The VAMP8/STX8 ratio was calculated for the indicated lanes and shown as mean and standard error (normalized relative to WT, which was set to 100%). Differences that were statistically significant from WT as determined by student's T test are indicated by (*). Exact *p* value: $p = 0.0009$. Numbers and tick marks left of blots indicate position and size (in kilodaltons) of protein standard in ladder. The (#) symbol denotes the presence of light chain immunoglobulin. Immunoblots were performed independently three times, and a representative example is shown. Ig; immunoglobulin. IP; immunoprecipitation. EV; Empty Vector. WT; wild-type. PCC; Pearson's Correlation Coefficient.

Figure 6: IFITM3 inhibits assembly of late endosome homotypic fusion machinery and promotes the delivery of endosomal cargo to lysosomes. (A) HEK293T stably expressing Empty Vector, IFITM3 WT-FLAG, or IFITM3 G95L-FLAG were co-transfected with STX7-HA, STX8-HA, Vti1b-HA, and VAMP8-Myc. Following whole cell lysis, samples were either boiled at 100°C (+) or not (-). SDS-PAGE and immunoblotting was performed with anti-Myc and anti-FLAG. Actin was used as loading control. Numbers and tick marks left of blots indicate position and size (in kilodaltons) of protein standard in ladder. Immunoblots were performed independently twice, and a representative example is shown. (B) HEK293T cells stably expressing Empty Vector, IFITM3 WT-FLAG, or IFITM3 G95L-FLAG were pulsed with

Dextran Alexa Fluor 488 for 2 hrs followed by addition of Magic Red for 5 mins. Living cells were then analyzed immediately by confocal immunofluorescence microscopy. Colocalization between Dextran and Magic Red was measured by calculating the Pearson's Correlation Coefficient using Fiji software. Coefficients were calculated from medial Z-slices from three fields of view containing 5-15 cells per condition and presented as means and standard error. Scale bar = 15 microns. PCC; Pearson's Correlation Coefficient.

Figure 7: IFITM3 traffics incoming IAV to lysosomes in a G95-dependent manner.
(A) HEK293T cells stably expressing Empty Vector, IFITM3 WT-FLAG, or IFITM3 G95L-FLAG inoculated with IAV at a multiplicity of infection of 1 and incubated on ice for 40 minutes. Cells were washed, fresh medium containing Lysotracker Deep Red (50 nM) was added, and cells were placed at 37°C for 4 hours. Four hours later, cells were fixed and immunostained with anti-NP antibody and Hoechst and analyzed by confocal immunofluorescence microscopy. Mock-inoculated (PBS) Empty Vector cells were used as a negative control. Scale bar = 15 microns. Medial Z-slices representative of each condition are shown. (B) The percentage of NP+ nuclei was quantified in Empty Vector, IFITM3 WT-FLAG, or IFITM3 G95L-FLAG cells. Symbols represent fields of view containing approximately 15-30 total cells and mean percentage plus standard error is shown. Differences that were statistically significant between the indicated conditions as determined by one-way ANOVA are indicated by (*). Exact p values are as follows (from left to right): $p < 0.0001$, $p = 0.0028$. (C) The Corrected Total Cell Fluorescence (CTCF) intensity of Lysotracker staining was quantified in Empty Vector, IFITM3 WT-FLAG, or IFITM3 G95L-FLAG cells. Symbols represent fields of view containing approximately 15-30 total cells and mean CTCF intensity plus standard error is shown. Differences that were statistically significant between the indicated conditions as determined by one-way ANOVA are indicated by (*). Exact p values are as follows (from left to right): $p = 0.0005$, $p = 0.0001$. (D) Examination of NP signal in relation to Lysotracker staining in HEK293T stabling expressing IFITM3 WT-FLAG or IFITM3 G95L-FLAG. White boxes indicate fields of view selected for detailed analysis. Right: detailed view of three different Z slices from confocal stack. White boxes indicate fields of view selected for further detailed analysis. White arrows indicate bright NP puncta that colocalize with Lysotracker or which tightly appose a Lysotracker+ compartment. Colocalization between NP and Lysotracker was measured by calculating the Pearson's Correlation Coefficient using Fiji software. Coefficients were calculated from medial Z-slices from three fields of view containing 5-15 cells per condition and presented as means plus standard deviation. Scale bar = 15 microns. EV; Empty Vector. WT; wild-type. hpi; hours post-inoculation. CTCF; Corrected Total Cell Fluorescence. PCC; Pearson's Correlation Coefficient.

Figure 8: A model of inhibition of homotypic late endosome fusion by IFITM3.
IFITM3 selectively regulates the trans-SNARE assembly driving late endosome-late endosome fusion (STX7-STX8-Vti1b-VAMP8), while enabling late endosome-lysosome fusion. As a result, endocytic cargos (including viruses) are more efficiently trafficked to lysosomes in IFITM3-expressing cells. LE; late endosome. Lys; lysosome.

Expanded View Figure Legends

Figure EV1: An R-SNARE-like motif is semi-conserved among human CD225 family members.

(A) Human CD225 proteins were aligned and trimmed to a 53-residue stretch of sequence covering the SNARE motif. Proteins are grouped by whether they contain an arginine at the central "0" layer (R-SNARE-like) or not. Surrounding heptad repeats of hydrophobic residues are labeled from "-7" to "+8" in relation to the "0" layer, and sites highlighted in yellow correspond to hydrophobic residues. (B) Left: HEK293T cells were co-transfected with STX1A-HA and either PRRT2-FLAG (WT, R295Q, G305W, or A320V) or Empty Vector. SDS-PAGE and immunoblotting were performed with anti-HA and anti-FLAG in whole cell lysates. Anti-actin was used as loading control. Right: From co-transfected cells, STX1A-HA was immunoprecipitated with anti-HA followed by SDS-PAGE and immunoblotting with anti-HA and anti-FLAG. Immunoglobulin chain was used as loading control. (C) Left: HEK293T cells were co-transfected with STX4-HA and either TUSC5-FLAG (WT or G141W) or Empty Vector. SDS-PAGE and immunoblotting were performed with anti-HA and anti-FLAG in whole cell lysates. Anti-actin was used as loading control. Right: From co-transfected cells, TUSC5-FLAG was immunoprecipitated with anti-FLAG followed by SDS-PAGE and immunoblotting with anti-HA and anti-FLAG. Light chain immunoglobulin chain was used as loading control. The HA/FLAG ratio was calculated for the indicated lanes and shown as mean and standard error (normalized relative to WT, which was set to 100%). Differences that were statistically significant from WT as determined by student's T test are indicated by (*). Exact p value: $p < 0.0001$. (D) From co-transfected cells, STX4-HA was immunoprecipitated with anti-HA followed by SDS-PAGE and immunoblotting with anti-FLAG and anti-HA. Light chain immunoglobulin was used as loading control. Numbers and tick marks left of blots indicate position and size (in kilodaltons) of protein standard in ladder. Immunoblots were performed independently three times, and a representative example is shown (except for (D), which was performed twice). Ig; immunoglobulin. IP; immunoprecipitation. EV; Empty Vector. WT; wild-type.

Figure EV2: IFITM3 contains a motif resembling the alpha helical R-SNARE motif of VAMP8

(A) The R-SNARE-like motif of IFITM3 and the R-SNARE motif of VAMP8 (53 residues each) were compared by predictive protein structure alignment and comparison algorithm TM-align. A TM score of 0.75847 was recorded, indicating that the two regions are likely to adopt the same alpha helical protein fold. (B) Structural prediction of the R-SNARE-like motif of IFITM3 was performed with Alphafold and FATCAT. Residues 55-113 of IFITM3 were modeled against a template of the R-SNARE motif of VAMP8 which was previously crystallized as part of the STX7-STX8-Vti1b-VAMP8 trans-SNARE complex (PDB: 1GL2). VAMP8 was then swapped with the predicted structure of IFITM3 and shown in relation to the coiled-coiled structure formed with STX7, STX8, and Vti1b. Top: the side chains of residues F75, F78, and R85 of IFITM3 are depicted in yellow and labeled. Bottom: alternative view of the side chains of F75, F78, and R85 of IFITM3. (C) Top: examination of the central polar "0" layer of the Q-SNAREs STX7, STX8, Vti1b in relation to the R85 residue in the predicted configuration of IFITM3. Bottom: examination of the central polar "0" layer of the STX7-STX8-Vti1b-VAMP8 complex (PDB: IGL2).

Figure EV3: IFITM3 interacts with the R-SNAREs VAMP8 and VAMP7

(A) Left: HEK293T cells were co-transfected with VAMP8-HA and IFITM3-FLAG (WT or G95L). SDS-PAGE and immunoblotting were performed with anti-HA and anti-FLAG in whole cell lysates. Anti-actin was used as loading control. Right: From co-transfected cells, VAMP8-HA was immunoprecipitated with anti-HA followed by SDS-PAGE and immunoblotting with anti-HA and anti-FLAG. Light chain immunoglobulin chain was used as loading control. The FLAG/HA ratio was calculated for the indicated lanes and shown as mean and standard error (normalized relative to WT, which was set to 100%). Differences that were statistically significant from WT as determined by student's T test are indicated by (*). Exact *p* value: $p < 0.0001$. (B) Left: HEK293T cells were co-transfected with VAMP7-myc and IFITM3-FLAG (WT or G95L). SDS-PAGE and immunoblotting were performed with anti-myc and anti-FLAG in whole cell lysates. Anti-actin was used as loading control. Right: From co-transfected cells, VAMP7-myc was immunoprecipitated with anti-myc followed by SDS-PAGE and immunoblotting with anti-myc and anti-FLAG. Light chain immunoglobulin chain was used as loading control. The FLAG/Myc ratio was calculated for the indicated lanes and shown as mean and standard error (normalized relative to WT, which was set to 100%). Differences that were statistically significant from WT as determined by student's T test are indicated by (*). Exact *p* value: $p = 0.0023$. Numbers and tick marks left of blots indicate position and size (in kilodaltons) of protein standard in ladder. Immunoblots were performed independently three times, and a representative example is shown. Ig; immunoglobulin. IP; immunoprecipitation. WT; wild-type.

Figure EV4: IFITM3 does not impair the STX7/STX8 or STX7/Vti1b interactions

(A) HeLa cells (WT or *IFITM3* KO) were subjected to whole cell lysis, SDS-PAGE, and immunoblotting with anti-IFITM2/3, anti-STX8, anti-Vti1b, anti-VAMP8, anti-VAMP7, and anti-actin. Red and green arrows indicate IFITM3 and IFITM2, respectively, recognized by the anti-IFITM2/3 antibody. (B) STX7-HA was transfected into HeLa (WT or *IFITM3* KO) and immunoprecipitated with anti-HA followed by SDS-PAGE and immunoblotting with anti-HA, anti-IFITM3, anti-STX8, and anti-Vti1b. Heavy chain immunoglobulin was used as loading control. An isotype matched antibody was used as a control for immunoprecipitation. The (#) symbol denotes the presence of light chain immunoglobulin. (C) Purified recombinant IFITM3 protein (WT, F75/78A, or G95L) of varying inputs (6, 12 or 18 µg) were subjected to SDS-PAGE and visualized by Coomassie stain. (D) 20 ng of purified recombinant IFITM3 protein (WT, F75/78A, or G95L) were subjected to SDS-PAGE and immunoblotting with anti-IFITM3. (E) Recombinant STX7 of varying inputs (0.5, 1, or 2 µg) were subjected to SDS-PAGE and visualized by Coomassie stain. (F) Recombinant STX7 was subjected to SDS-PAGE and immunoblotting with anti-STX7. Numbers and tick marks left of blots indicate position and size (in kilodaltons) of protein standard in ladder. Immunoblots were performed independently two times and a representative example is shown (for (A) and (B)) or once (for (C), (D), (E), and (F)). Ig; immunoglobulin. IP; immunoprecipitation. EV; Empty Vector. WT; wild-type. r; recombinant.

Figure EV5: IFITM3 does not impair the STX7/VAMP7 interaction

(A) Size exclusion chromatography was performed on recombinant IFITM3 proteins (WT, F75/78A, and G95L) and eluted fractions were analyzed by SDS-PAGE and Coomassie staining. 150 µg recombinant protein was loaded as input and fraction numbers correspond to mL volumes eluted from column. (B) Left: HEK293T cells stably expressing Empty Vector, IFITM3 WT-FLAG, or IFITM3 G95L-FLAG were co-transfected with STX7-HA and VAMP7-Myc. Whole

cell lysates were subjected to SDS-PAGE and immunoblotting with anti-HA, anti-FLAG, and anti-Myc. Actin was used as a loading control. Right: STX7-HA was immunoprecipitated with anti-HA followed by SDS-PAGE and immunoblotting with anti-HA, anti-FLAG, and anti-Myc. The Myc/HA ratio was calculated for the indicated lanes and shown as mean and standard error (normalized relative to Empty Vector, which was set to 100%). Differences that were statistically significant from Empty Vector as determined by one-way ANOVA are indicated by (*). Exact p values are as follows (from left to right): $p = 0.0099$, $p = 0.8782$. Numbers and tick marks left of blots indicate position and size (in kilodaltons) of protein standard in ladder. Immunoblots were performed independently three times, and a representative example is shown (except (A), which was performed once). (C) HeLa (WT or *IFITM3* KO) were transfected with STX7-GFP and VAMP8-mCherry and confocal immunofluorescence microscopy was performed. Colocalization between STX7-GFP and VAMP8-mCherry was measured by calculating the Pearson's Correlation Coefficient using Fiji software. Coefficients were calculated from medial Z-slices from three fields of view containing 5-15 cells per condition and presented as means and standard error. Scale bar = 15 microns. IP; immunoprecipitation. WT; wild-type. r; recombinant.

A

```
                -7 -6  -5 -4  -3 -2  -1  0  +1 +2  +3 +4  +5 +6  +7 +8
Syntaxin 1a     IIKLENSIRELHDMFMDMAMLVESQGEMIDRIEYNVEHAVDYVERAVSDTKKA
Syntaxin 4      IQQLERSIRELHDIFTFLATEVEMQGEMINRIEKNILSSADYVERGQEHVKTA
Syntaxin 6      LELVSGSIGVLKNMSQRIGGELEEQAVMLEDFSHELESTQSRLDNVMKKLAKV
Syntaxin 7      IRQLEADIMDINEIFKDLGMMIHEQGDVIDSIEANVENAEVHVQQANQQLSRA
Syntaxin 8      LDALSSIISRQKQMGQEIGNELDEQNEIIDDLANLVENTDEKLRNETRRVNMV
Vti1a           LEAGYQIAVETEQIGQEMLENLSHDREKIQRARERLRETDANLGKSSRILTGM
Vti1b           IERSHRIATETDQIGSEIIEELGEQRDQLERTKSRLVNTSENLSKSRKILRSM
SNAP-25         TRRMLQLVEESKDAGIRTLVMLDEQGEQLERIEEGMDQINKDMKEAEKNLTDL
Syn8P (Sc)      LGALSQSIGRTHDISLDLNNEIVSQNDSLLVDLENLIDNNGRNLNRASRSMHG
VAMP1           LQQTQAQVEEVVDIIRVNVDKVLERDQKLSELDDRADALQAGASQFESSAAKL
VAMP2           LQQTQAQVDEVVDIMRVNVDKVLERDQKLSELDDRADALQAGASQFETSAAKL
VAMP3           LQQTQNQVDEVVDIMRVNVDKVLERDQKLSELDDRADALQAGASQFETSAAKL
VAMP5           LERCQQQANEVTEIMRNNFGKVLERGVKLAELQQRSDQLLDMSSTFNKTTQNL
VAMP7           VMETQAQVDELKGIMVRNIDLVAQRGERLELLIDKTENLVDSSVTFKTTSRNL
VAMP8           VRNLQSEVEGVKNIMTQNVERILARGENLEHLRNKTEDLEATSEHFKTTSQKV
YKT6            MTKVQAELDETKIILHNTMESLLERGEKLDDLVSKSEVLGTQSKAFYKTARKQ
Tomosyn         IEGVKGAASGVVGELARARLALDERGQKLGDLEERTAAMLSSAESFSKHAHEI
Amisyn          NSILHSAADSVTSAVQKASQALNERGERLGRAEEKTEDLKNSAQQFAETAHKL
IFITM1          SLFNTLFLNWCCLGFIAFAYSVKSRDRKMVGDVTGAQAYASTAKCLNIWALIL
IFITM2          SLFNTLFMNTCCLGFIAFAYSVKSRDRKMVGDVTGAQAYASTAKCLNIWALIL
IFITM3       55 SLFNTLFMNPCCLGFIAFAYSVKSRDRKMVGDVTGAQAYASTAKCLNIWALIL 113
TUSC5       108 LAVVACFCPVWPLNLIPLIISIMSRSSMQQGNVDGARRLGRLARLLSITLIIM 159
PRRT2       271 LAILSCFCPMWPVNIVAFAYAVMSRNSLQQGDVDGAQRLGRVAKLLSIVALVG 323
```

Q-SNARE

R-SNARE

R-SNARE-like

CD225

B

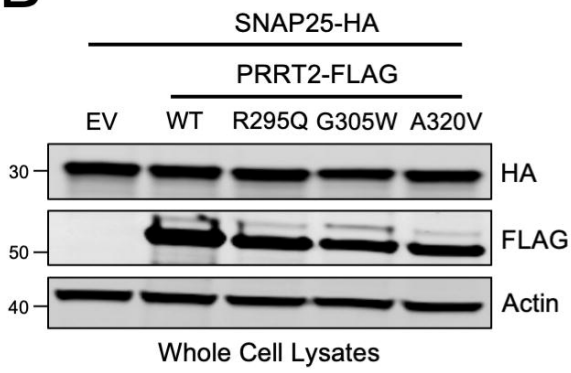

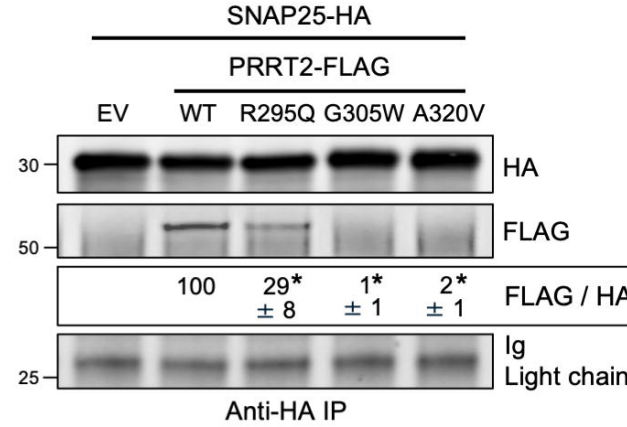

A

```
                -7 -6  -5 -4  -3 -2  -1  0  +1 +2  +3 +4  +5 +6  +7 +8
Syntaxin 7      IRQLEADIMDINEIFKDLGMMIHEQGDVIDSIEANVENAEVHVQQANQQLSRA
Syntaxin 8      LDALSSIISRQKQMGQEIGNELDEQNEIIDDLANLVENTDEKLRNETRRVNMV
     Vti1b      IERSHRIATETDQIGSEIIEELGEQRDQLERTKSRLVNTSENLSKSRKILRSM
     VAMP8      VRNLQSEVEGVKNIMTQNVERILARGENLEHLRNKTEDLEATSEHFKTTSQKV
     VAMP7      VMETQAQVDELKGIMVRNIDLVAQRGERLELLIDKTENLVDSSVTFKTTSRNL

    IFITM1      SLFNTLFLNWCCLGFIAFAYSVKSRDRKMVGDVTGAQAYASTAKCLNIWALIL
    IFITM2      SLFNTLFMNTCCLGFIAFAYSVKSRDRKMVGDVTGAQAYASTAKCLNIWALIL
    IFITM3   55 SLFNTLFMNPCCLGFIAFAYSVKSRDRKMVGDVTGAQAYASTAKCLNIWALIL 113
```

B

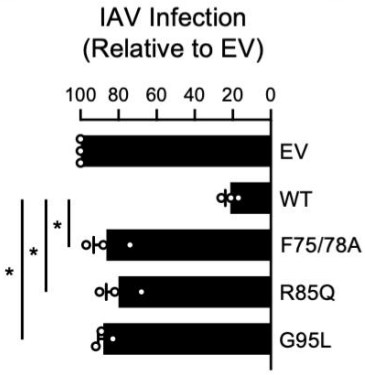

C

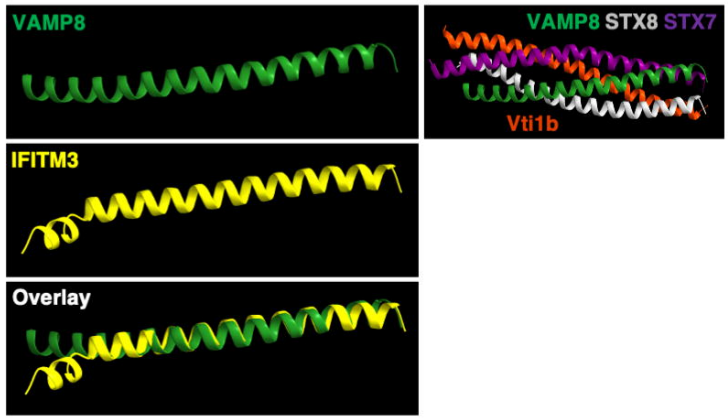

D

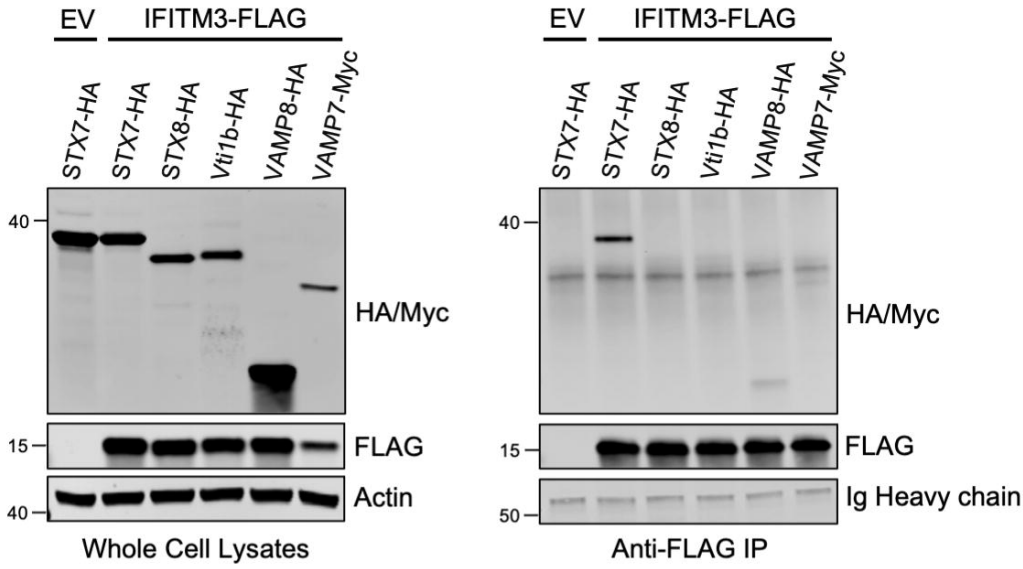

E

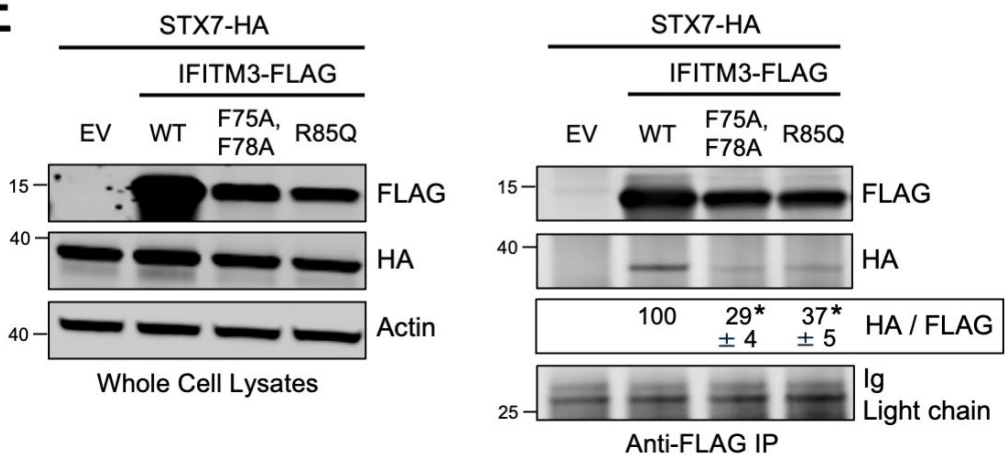

A

STX8-HA | STX7-HA | Vti1b-HA

EV | IFITM3-FLAG | IFITM3-FLAG | IFITM3-FLAG

WT | F75A, F78A | G95L | WT | F75A, F78A | G95L | WT | F75A, F78A | G95L

40 — HA

15 — FLAG

50 — Tubulin

Whole Cell Lysates

STX8-HA | STX7-HA | Vti1b-HA

EV | IFITM3-FLAG | IFITM3-FLAG | IFITM3-FLAG

WT | F75A, F78A | G95L | WT | F75A, F78A | G95L | WT | F75A, F78A | G95L

40 — HA

15 — FLAG

FLAG / HA: 12* ± 5 | 4* ± 2 | 1* ± 1 | 100 | 30* ± 5 | 16* ± 4

50 — Ig Heavy chain

Anti-HA IP

B

STX7-GFP

Empty Vector | IFITM3-FLAG WT | IFITM3-FLAG G95L

STX7-GFP

FLAG

Merge

STX7 / FLAG PCC = 0.580 ± 0.066

STX7 / FLAG PCC = 0.155 ± 0.065

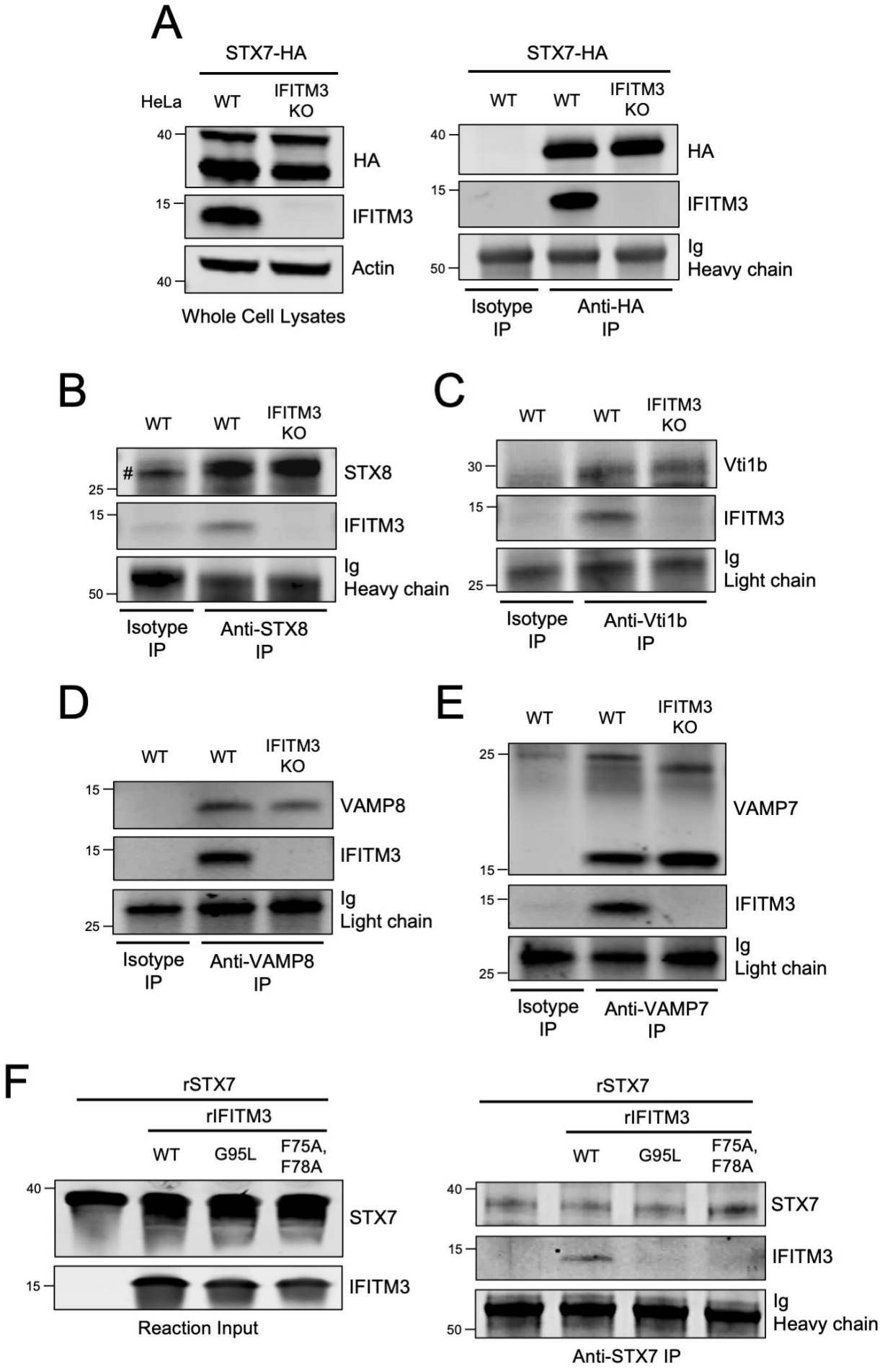
A
STX7-HA
HeLa
WT
IFITM3 KO
40
HA
15
IFITM3
Actin
40
Whole Cell Lysates
STX7-HA
WT
WT
IFITM3 KO
40
HA
15
IFITM3
Ig Heavy chain
50
Isotype IP
Anti-HA IP
B
WT
WT
IFITM3 KO
#
STX8
25
15
IFITM3
Ig Heavy chain
50
Isotype IP
Anti-STX8 IP
C
WT
WT
IFITM3 KO
30
Vti1b
15
IFITM3
Ig Light chain
25
Isotype IP
Anti-Vti1b IP
D
WT
WT
IFITM3 KO
15
VAMP8
15
IFITM3
Ig Light chain
25
Isotype IP
Anti-VAMP8 IP
E
WT
WT
IFITM3 KO
25
VAMP7
15
15
IFITM3
Ig Light chain
25
Isotype IP
Anti-VAMP7 IP
F
rSTX7
rIFITM3
WT
G95L
F75A, F78A
40
STX7
15
IFITM3
Reaction Input
rSTX7
rIFITM3
WT
G95L
F75A, F78A
40
STX7
15
IFITM3
Ig Heavy chain
50
Anti-STX7 IP

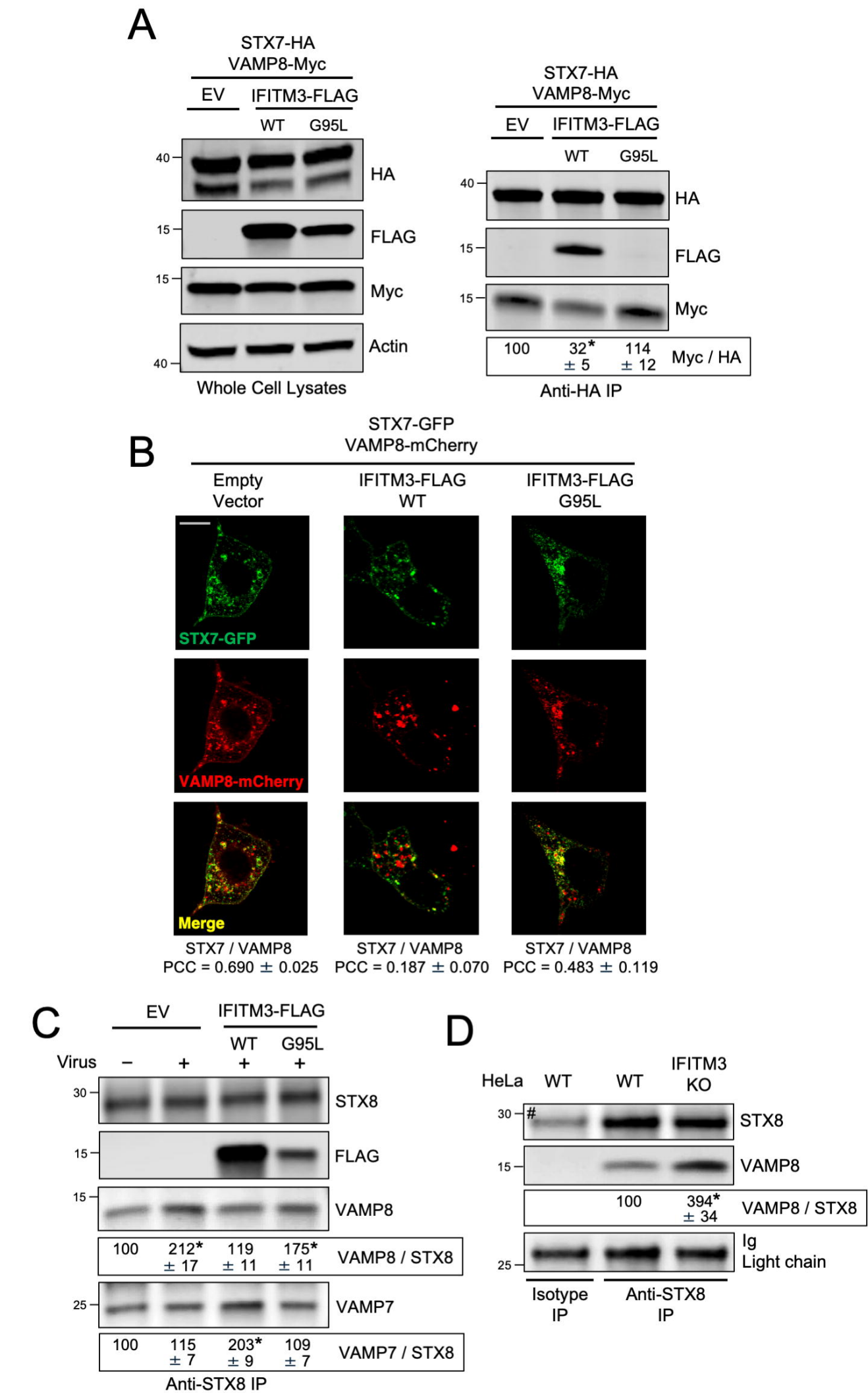
A
STX7-HA
VAMP8-Myc
EV
IFITM3-FLAG
WT
G95L
40
HA
15
FLAG
15
Myc
Actin
40
Whole Cell Lysates
STX7-HA
VAMP8-Myc
EV
IFITM3-FLAG
WT
G95L
40
HA
15
FLAG
15
Myc
100
32*
± 5
114
± 12
Myc / HA
Anti-HA IP
B
STX7-GFP
VAMP8-mCherry
Empty Vector
IFITM3-FLAG WT
IFITM3-FLAG G95L
STX7-GFP
VAMP8-mCherry
Merge
STX7 / VAMP8
PCC = 0.690 ± 0.025
STX7 / VAMP8
PCC = 0.187 ± 0.070
STX7 / VAMP8
PCC = 0.483 ± 0.119
C
EV
IFITM3-FLAG
WT
G95L
Virus
–
+
+
+
30
STX8
15
FLAG
15
VAMP8
100
212*
± 17
119
± 11
175*
± 11
VAMP8 / STX8
25
VAMP7
100
115
± 7
203*
± 9
109
± 7
VAMP7 / STX8
Anti-STX8 IP
D
HeLa
WT
WT
IFITM3 KO
30
#
STX8
15
VAMP8
100
394*
± 34
VAMP8 / STX8
25
Ig Light chain
Isotype IP
Anti-STX8 IP

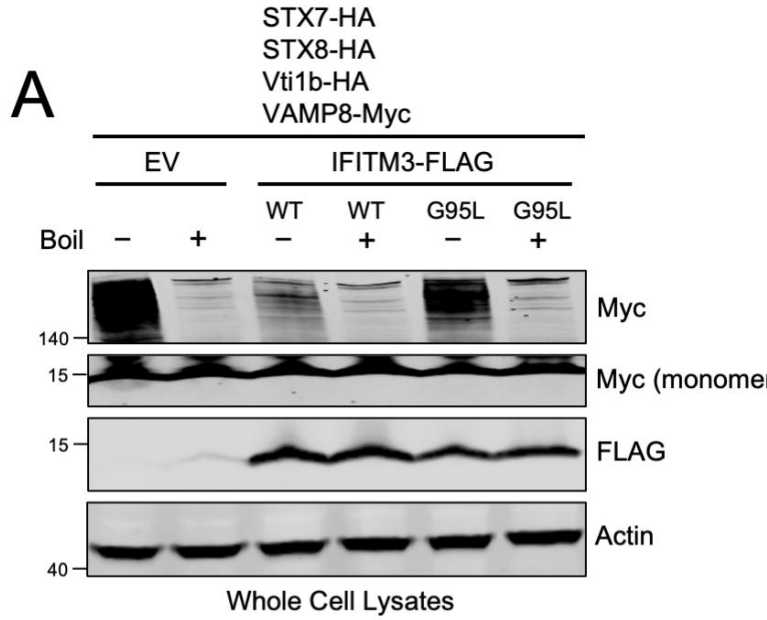
A
STX7-HA
STX8-HA
Vti1b-HA
VAMP8-Myc
EV
IFITM3-FLAG
WT
WT
G95L
G95L
Boil
−
+
−
+
−
+
140
15
15
40
Myc
Myc (monomer)
FLAG
Actin
Whole Cell Lysates

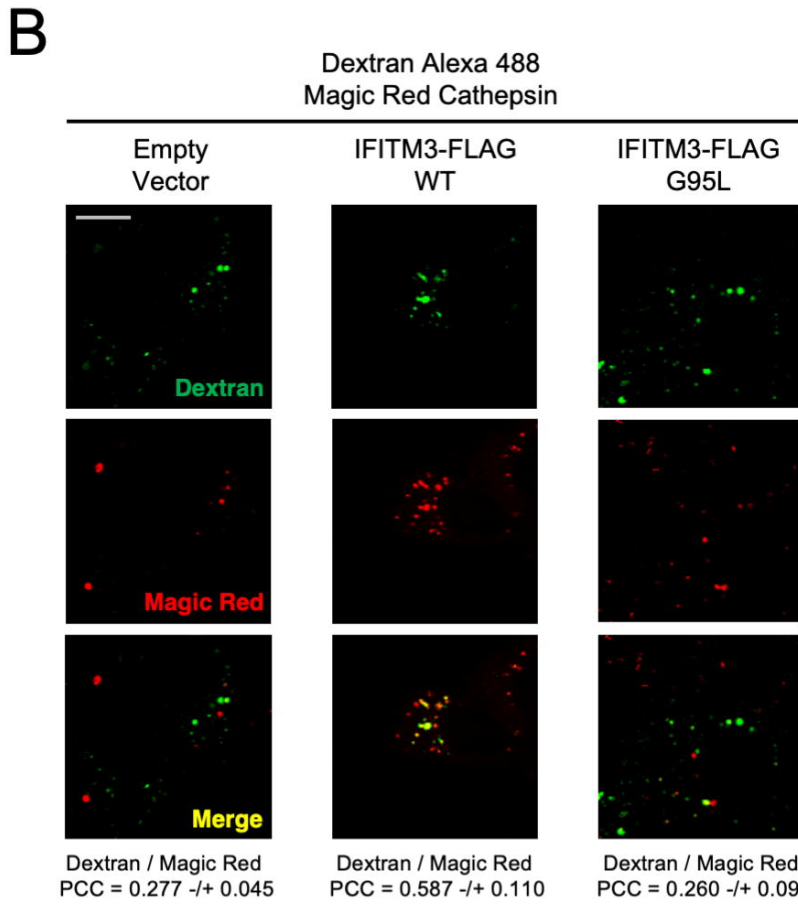
B
Dextran Alexa 488
Magic Red Cathepsin
Empty Vector
IFITM3-FLAG WT
IFITM3-FLAG G95L
Dextran
Magic Red
Merge
Dextran / Magic Red
PCC = 0.277 -/+ 0.045
Dextran / Magic Red
PCC = 0.587 -/+ 0.110
Dextran / Magic Red
PCC = 0.260 -/+ 0.095

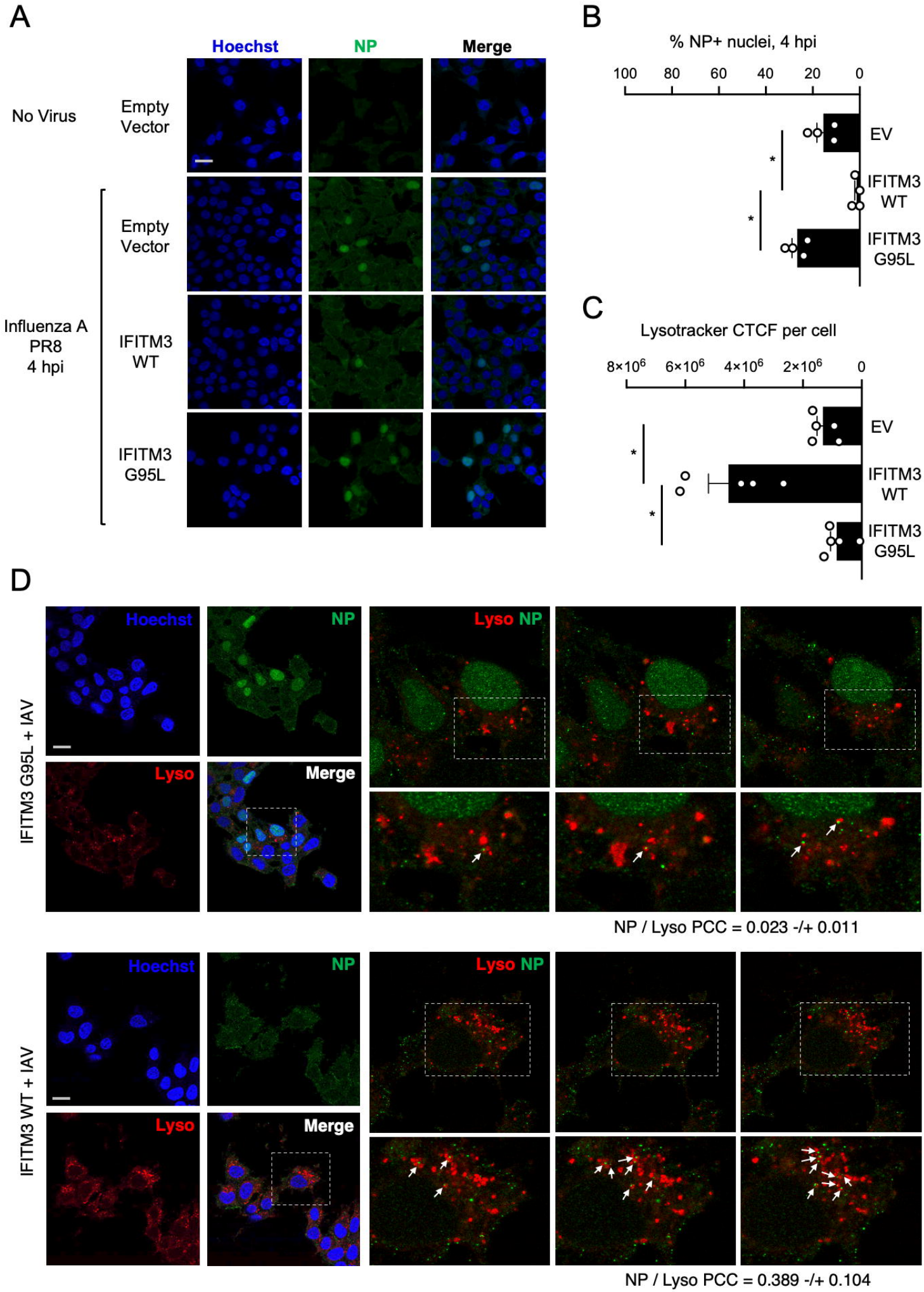
A
Hoechst
NP
Merge
No Virus
Empty Vector
Influenza A PR8 4 hpi
Empty Vector
IFITM3 WT
IFITM3 G95L
B
% NP+ nuclei, 4 hpi
100
80
60
40
20
0
EV
IFITM3 WT
IFITM3 G95L
*
*
C
Lysotracker CTCF per cell
8×10^6
6×10^6
4×10^6
2×10^6
0
EV
IFITM3 WT
IFITM3 G95L
*
*
D
IFITM3 G95L + IAV
Hoechst
NP
Lyso NP
Lyso
Merge
NP / Lyso PCC = 0.023 -/+ 0.011
IFITM3 WT + IAV
Hoechst
NP
Lyso NP
Lyso
Merge
NP / Lyso PCC = 0.389 -/+ 0.104

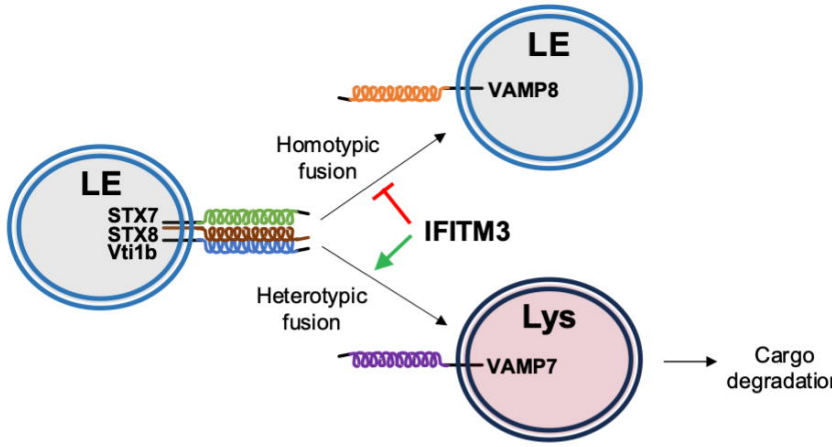
LE
VAMP8
Homotypic
fusion
LE
STX7
STX8
Vti1b
IFITM3
Heterotypic
fusion
Lys
VAMP7
Cargo
degradation